Chem Soc Rev

Cite this: *Chem. Soc. Rev.*, 2012, **41**, 2283–2307

www.rsc.org/csr

CRITICAL REVIEW

Biological and chemical sensors based on graphene materials

Yuxin Liu, Xiaochen Dong and Peng Chen*

Received 27th September 2011
DOI: 10.1039/c1cs15270j

Owing to their extraordinary electrical, chemical, optical, mechanical and structural properties, graphene and its derivatives have stimulated exploding interests in their sensor applications ever since the first isolation of free-standing graphene sheets in year 2004. This article critically and comprehensively reviews the emerging graphene-based electrochemical sensors, electronic sensors, optical sensors, and nanopore sensors for biological or chemical detection. We emphasize on the underlying detection (or signal transduction) mechanisms, the unique roles and advantages of the used graphene materials. Properties and preparations of different graphene materials, their functionalizations are also comparatively discussed in view of sensor development. Finally, the perspective and current challenges of graphene sensors are outlined (312 references).

1. Introduction

Graphene is a single-atom-thick planar sheet of sp^2-bonded carbon atoms perfectly arranged in a honeycomb lattice. Owing to its extraordinary physicochemical and structural properties,[1–5] this exciting new material has quickly sparked tremendous interests across many disciplines, including nanoelectronics and high-frequency electronics,[6–8] energy storage and conversion,[9,10] field emission display,[11,12] and transparent conductors.[13] In this article, we survey the emerging applications of graphene for biological and chemical sensing.

Division of Bioengineering, School of Chemical and Biomedical Engineering, Nanyang Technological University, Singapore 637457, Singapore. E-mail: chenpeng@ntu.edu.sg

In the past decade or so, various zero dimensional (0D) and one dimensional (1D) nanomaterials have been the main impetus for novel and better sensor developments.[14–17] These include quantum dots,[18,19] nanoparticles,[20,21] nanowires,[22–25] and notably, carbon nanotubes[26–29] that are one-dimensional cylinders of carbon sheets. Ever since the first isolation of free-standing graphene sheets in 2004,[30] this two-dimensional (2D) carbon crystal has been highly anticipated to provide unique and new opportunities for sensor applications. In fact, despite its short history, graphene has already demonstrated great potentials in various novel sensors which utilize graphene's exceptional electrical properties (*e.g.*, extremely high carrier mobility and capacity), electrochemical properties (*e.g.*, high electron transfer rate), optical properties (*e.g.*, excellent ability to quench fluorescence), structural properties

Yuxin Liu

Yuxin Liu (born in 1990) is currently a junior student in the Division of Bioengineering at Nanyang Technological University (Singapore). He is the welfare director of Student Union in the School of Chemical & Biomedical engineering and participating in the URECA undergraduate research program under the supervision of Prof. Peng Chen. His current research interests are biosensors and bionanotechnology.

Peng Chen

Peng Chen is currently an Associate Professor of Bioengineering in School of Chemical and Biomedical Engineering at Nanyang Technological University (Singapore). He completed his PhD in University of Missouri (Columbia) in 2002. This was followed by a period of postdoctoral research at Harvard University. His research interests are in the areas of nanomaterials, biosensors, and bionanotechnology. He is particularly interested in applying interdisciplinary and integrative approaches to study biomedical problems.

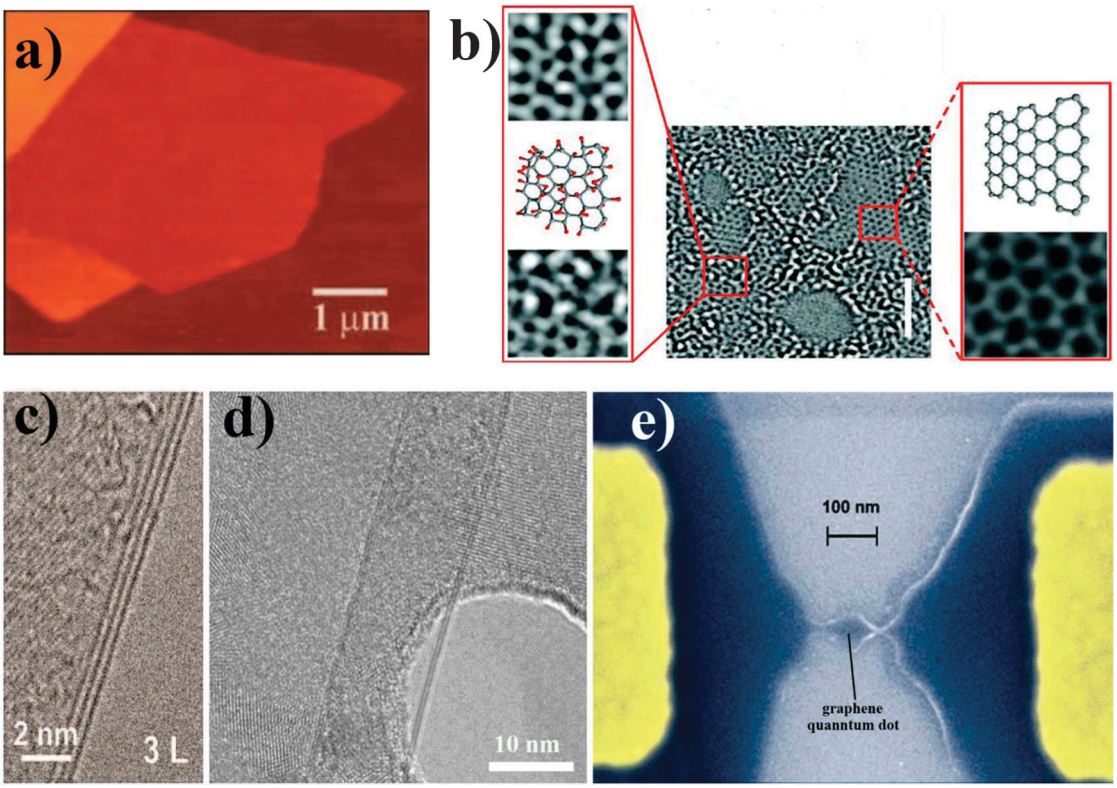

Fig. 1 Different graphene materials. (a) Atomic force microscopy (AFM) image of a single-layer graphene obtained by mechanical cleavage of graphite. Adapted with permission from ref. 30. Copyright 2004 *Science*. (b) Aberration-corrected transmission electron microscopy (TEM) image of a single sheet of suspended graphene oxide. The scale bar is 2 nm. Left expansion shows, from top to bottom, a 1 nm^2 enlarged oxidized region of the material, then a proposed atomic structure of this region with carbon atoms in gray and oxygen atoms in red, and finally the average of a simulated TEM image of the proposed structure and a simulated TEM image of another structure where the position of oxidative functionalities has been changed. Right expansion shows a 1 nm^2 graphitic portion from the exit plane wave reconstruction of a focal series of GO and the atomic structure of this region. Adapted with permission from ref. 59. Copyright 2010 Wiley-VCH Verlag GmbH & Co. KGaA, Weinheim. (c) High magnification TEM image showing the edges of film regions consisting of 3 layers of CVD grown graphene. The cross-sectional view is enabled by the folding of the film edge. Adapted with permission from ref. 43. Copyright 2009 American Chemical Society. (d) TEM image of a graphene nanoribbon suspended over porous silicon grids, showing nearly atomically smooth edges. Adapted with permission from ref. 70. Copyright 2009 American Chemical Society. (e) The scanning electron micrograph (in false color) illustrates a graphene quantum dot device. Adapted with permission from ref. 83. Copyright 2008 *Science*.

(*e.g.*, one-atom thickness and extremely high surface-to-volume ratio), or its mechanical properties (*e.g.*, outstanding robustness and flexibility).

Although graphene has also been used as physical sensors (*e.g.*, for detection of photons,[31] magnetic field,[32] mass[33,34] and strain),[35] here, we place the emphases on biological and chemical sensors. We aim to provide a comprehensive review covering the latest developments, and importantly, offer insights on the underlying detection mechanisms and on the unique advantages of graphene in comparison with other materials. We hope that this article would inspire broader interests across various disciplines and stimulate more exciting developments in this still young yet very promising field of research.

2. Properties and preparations of graphene materials

Different synthetic routes produce graphene materials with distinct characteristics. In this section, we briefly discuss these preparation methods and the properties of the resulting graphene materials in a comparative way. This discussion shall provide clues for optimal selection of a graphene material for a particular sensor development and help to understand the advantages and disadvantages of the chosen material.

A single-layer graphene (SLG) sheet was first obtained by mechanical cleavage of graphite (Fig. 1a).[30] The high quality pristine graphene sheet obtained in this way is a fascinating model system for condensed-matter physics and has allowed physicists to reveal the fundamental properties of this amazing material. The pristine SLG is a semi-metal with zero energy bandgap. It exhibits remarkably high carrier mobility at room temperature (20 000 $cm^2\ V^{-1}\ s^{-1}$),[36] high carrier density ($10^{13}\ cm^{-2}$),[36] room temperature Hall effect,[37] low intrinsic noises as compared with other nanostructured materials,[38–40] and ambipolar field-effect characteristics. These exceptional properties are particularly useful for the development of electronic sensors. However, mechanical exfoliation is of low throughput and not able to produce a large-sized graphene sheet (typically, limited to a few micrometres). These drawbacks greatly limit the practical use of mechanically exfoliated graphene.

A graphene film can be grown on transition metal substrates (*e.g.*, nickel, copper, palladium) using chemical vapor

deposition (CVD) (Fig. 1c).[41–43] At low pressure, the CVD growth of graphene on copper foil is a self-limiting process, *i.e.*, it automatically stops after a single graphene layer forms.[44] An advantage of CVD growth is that substitutional doping is feasible by introducing heteroatoms (nitrogen, boron, *etc.*) into the carbon lattice. The type and the extent of doping can be manipulated. In addition, CVD growth is able to produce large-sized graphene films which ease the sensor device fabrication and provide a large detection area. The properties of CVD grown graphene, however, deviate to some extent from that of the pristine SLG (*e.g.*, decrease in mobility and shift in the Dirac point), due to existence of defects, impurities, and few-layered domains. And the necessity to transfer the as-grown graphene film from the metal substrate to an insulating substrate for device fabrication usually introduces additional impurities and limits the actual attainable size for device fabrication.[45]

Another method to obtain an arbitrarily large graphene film is to decompose silicon carbide (SiC) to graphene at high temperatures.[46] An important advantage of this method is that a transfer process is not required because SiC itself is a good insulator. Therefore, large integrated circuits with hundreds of transistors can be carved on a single large-size epitaxial graphene on SiC using standard microelectronics technologies.[47] Conceivably, a sensor array with integrated amplification and processing circuits may be similarly made on an as-grown graphene film. An interesting phenomenon has been reported that the interaction between graphene and SiC substrate opens the graphene bandgap to $\sim$0.26 eV.[48] This is desired for field-effect transistors (FETs) and also for sensors whose detection relies on the induced field-effect. However, it is difficult to precisely control the properties of graphene epitaxially grown on SiC, which depend on the face of SiC used for graphene formation and the edge-termination (silicon or carbon). In addition, decomposition of SiC is not self-limiting. As a result, the resulting graphene film is heterogeneous in thickness (thus properties).

Chemical reduction of exfoliated graphene oxides (GO) was historically the first method for graphene synthesis, reported by Boehm and co-workers in 1962.[49] The interest of this method is greatly reignited after demonstration of the remarkable properties of mechanically exfoliated graphene, because it provides a facile route for low-cost mass-production of graphene, more accurately, reduced graphene oxide (RGO) or chemically derived graphene (CDG).[50] In addition to chemical reduction (most commonly, by hydrazine), RGO can also be obtained by thermal,[51] photothermal,[52] or electrochemical reduction.[53] Nevertheless, the properties of RGO are substantially different from that of pristine graphene, due to the defects in the sp^2 hybridized carbon lattice and a variety of oxygenated groups irreversibly caused by the oxidative process for chemical exfoliation of graphene oxides from graphite.[54] Although relativistic charge transport and some other condensed-matter effects observed in the pristine material are absent in RGO, its facile and scalable preparation, unique and tunable properties make it attractive for sensor applications. And the chemical groups on RGO provide convenient handles for surface modifications, for example, for covalent anchorage of the recognition elements against specific sensing targets. Since GO can dissolve in water and various solvents, solution-based processes (*e.g.*, inkjet printing, microfluidic patterning, spray-coating) together with *in situ* reduction can be employed to readily fabricate RGO thin-film devices on arbitrary substrates, for example, on a flexible substrate that can conformably attach onto a curved sensing object.[55] Moreover, RGO is more electrochemically active as compared to pristine graphene owing to the abundant reactive sites at edges and in a defective basal plane,[56] promising its use in electrochemical sensors.

Graphene oxide (GO), commonly obtained by placing graphite in a mixture of strong acid(s) and oxidizing agent(s),[57,58] not only is the precursor of RGO but also may serve as a sensing element itself. It is a heterogeneous, non-conductive, and atomically thin sheet with nano-sized sp^2 carbon clusters isolated by oxygenated sp^3 carbon domains (Fig. 1b).[50,59,60] In contrast to pristine graphene, GO is photoluminescent over a broad range of wavelengths due to quantum-confinement induced bandgap opening in the heterogeneously sized sp^2 clusters. On the other hand, GO is also a highly efficient fluorescence quencher. These optical properties suggest its potentials in optical detection.[61] The size, shape, composition, and relative fraction of sp^3-hybridized domains of GO can be chemically, thermally, or electrochemically engineered to manipulate GO's optoelectronic properties, for example, transforming it from an insulator to a semiconductor or to a graphene-like semi-metal.[60] RGO obtained from intense reduction of GO exhibits similar ambipolar characteristics with a low on-off ratio as that of pristine graphene, albeit with a much lower carrier mobility. RGO resulted from mild reduction can acquire a high on-off ratio because its transport is dominated by the voltage-dependent carrier tunneling or hopping between sp^2 clusters.[62] Such voltage dependent transport may be utilized for electronic sensing. Taken together, GO and RGO provide tunable, versatile and powerful platforms for various sensing applications. To preserve the crystalline carbon structure (hence the ballistic transport properties), graphene can be non-covalently exfoliated in the liquid phase, using molecules that can effectively intercalate between the stacked graphene layers in graphite.[63–66] But it should be kept in mind that those intercalating agents usually remain firmly associated with the graphene sheet and unavoidably alter its electronic structure.

The properties of graphene can be drastically modified or fine-tuned by atomistic or chemical doping.[67,68] Its properties also depend on its dimension, layer structure, and edge configuration. When one lateral dimension of graphene shrinks to nanoscale becoming graphene nanoribbons (GNRs), it may transform into a semiconductor with a large bandgap due to quantum confinement of the electron wave function.[69] GNRs can be obtained by longitudinally unzipping carbon nanotubes using gas-phase oxidation followed by sonication[70] (Fig. 1d), chemical attack by H_2SO_4 and $KMnO_4$,[71] lithium intercalation,[72] catalytic cutting by metal nanoparticles,[73] plasma etching on a carbon nanotube partially embedded in a polymeric matrix,[74] cutting by hydrogen,[75] electrochemical unzipping,[76] electrical unwrapping,[77] or laser cutting.[78] Alternatively, GNRs can be produced by templated growth on SiC,[79] surface-assisted bottom-up synthesis,[80] or top-down lithographic fabrication.[81] Two-dimensionally shrinking a graphene sheet to nanoscale results in a graphene quantum dot (GQD) which may operate as a single-electron transistor.[82] A GQD can be carved from

graphene using nanolithography[83,84] (Fig. 1e) or be produced by hydrothermal cleavage of GO.[85] Both GNRs and GQDs are highly sensitive to the field-effect and to chemical disruption at edges, therefore providing opportunities for ultrasensitive detection. In addition, their small dimensions permit spatially resolved or highly localized detection. Layer number is another important factor to influence the properties of graphene. It has been shown that, in contrast to zero bandgap single-layered graphene, bilayer graphene exhibits a continuously and widely tunable electronic bandgap up to 0.25 eV.[86]

As discussed above, the properties of graphene materials can be controlled by the synthetic conditions, dimensions, layer numbers, and doping. Such tunable and diverse properties of graphene materials provide vast possibilities for various sensing purposes. The selection of specific graphene material should be made according to the specific sensing target and the sensing mechanism to be utilized, with a balanced consideration on performance (*e.g.*, detection limit and dynamic range), reproducibility, cost, and manufacturability. In this article, for clarity, we sometimes generally refer all forms of graphene related materials as graphene in general discussions. But when sensor examples are discussed, the specific type of graphene material used will be unambiguously indicated (*e.g.*, mechanically exfoliated graphene, CVD grown graphene, RGO, GO, and so on). For more comprehensive information on graphene properties and preparations, the readers may consult the previous reviews and references therein.[67,87–93]

3. Graphene functionalization

To endow graphene with sensing capabilities, it is often necessary to functionalize it with recognition elements that bring the detection targets onto the graphene surface through specific interactions and sometimes also assist in signal transduction. Graphene may also be functionalized in order to enhance its sensitivity, specificity, loading capacity, biocompatibility, *etc*. Various strategies have been devised to functionalize graphene's 1D cousin, carbon nanotubes (CNTs).[94] These strategies could be adopted straightforwardly for graphene. As compared to the narrow CNTs (1–2 nm in diameter), 2D graphene is more amenable to effective, reproducible, and homogeneous functionalization. Here we briefly discuss the approaches to modify graphene and divide them into two general categories: covalent and noncovalent. For detailed chemistry, the readers may refer to several previous articles on this topic.[94–98]

3.1 Covalent methods

Chemical moieties, commonly, carboxylic (–COOH) and hydroxyl (–OH) groups, can be covalently created on the graphene surface using strong acids and/or oxidants. Exfoliated by an oxidation process, GO (also its reduced form –RGO) is populated with these oxygen-containing chemical groups. Fluorine, which is one of the strongest oxidants, can readily react with carbon materials including graphene. Different kinds of chemical moieties (*e.g.*, amino, hydroxyl, or alkyl groups) may then be introduced onto graphene by substituting the fluorine atoms due to the weak (highly reactive) C–F bonds in fluorinated graphene. In addition, microwave-assisted sulfonation has been used to create sulfonate ($-SO_3$) groups[99] while plasma (ammonia or nitrogen plasma) treatment has been used to create amino ($-NH_2$) groups on graphene.[100]

The chemical moieties created on the graphene surface can serve as chemical handles to graft functional molecules (*e.g.*, proteins, carbohydrates, polymers) through covalent bonding. For example, carboxylic groups can react with proteins, carbohydrates or other polymers *via* amide or ester linkages. Graphene may also be grafted with functional molecules containing a silane tail through salinization with hydroxyl groups on the graphene surface by forming an Si–O–C bond.[101] Functional molecules can be directly bonded on the graphene surface using free-radical addition, Billups reaction, cycloaddition, thermal or photochemical activated C=C addition, *etc*.[94,102,103] Covalent functionalization of linker molecules (*e.g.*, a branched polymer with multiple reactive ends) could be used to provide an amplification mechanism for further functionalization of sensing probes and/or to provide a spacing between graphene and sensing probes (or a sensing environment).[104]

3.2 Noncovalent methods

Although covalent strategies can effectively, stably and specifically install functionalities, they unavoidably alter the native electronic structure and physical properties of graphene by converting sp^2 carbons to sp^3 ones, *e.g.*, causing severe decrease in carrier mobility. In view of this problem, noncovalent modifications have been employed in order to preserve the intrinsic properties of the original graphene materials.

Various molecules can physically adsorb onto graphene materials without the need of any coupling reagents. Graphene can be viewed as a giant (the largest) aromatic molecule. It can firmly interact with any molecules with aromatic ring(s) on the surface. Graphene materials, for example, GO that is highly negatively charged, are able to electrostatically adsorb oppositely charged molecules. In addition, hydrophobic or van der Waals interaction may assist the physical adsorption. However, physical adsorption is non-specific. To deal with this issue, passivation molecules (commonly, bovine serum albumin and Tween-20) are often applied to block the unfunctionalized area (sites) in order to avoid non-specific adhesion of unwanted molecules. Similar passivation could also be used after covalent functionalizations to quench the un-reacted sites and block non-active area.[105]

Functional molecules can be immobilized onto graphene through linker molecules, for instance, 1-pyrenebutanoic acid succinimidyl ester whose pyrene group at one end noncovalently binds to the graphene surface through strong π–π interaction while the succinimidyl ester group at the other end is reactive to amines on biomolecules.[106] Other bifunctional molecules with an aromatic tail and a reactive end (*e.g.* perylene tetracarboxylic acid, thionine and many porphyrin derivatives) can also be employed as linker molecules.[98]

Graphene materials, particularly, GO and RGO, can be non-covalently decorated with metal nanoparticles (*e.g.*, Au, Ag, Pt) through *in situ* reduction,[107,108] electrospray[109] or electrochemical deposition.[110] These nanoparticles may serve as the catalysts to mediate signal transduction in graphene based sensors, or as the docking points to anchor sensing probes with high capacity. For instance, thiolated biomolecules

(*e.g.*, thiol-ssDNA) can be anchored onto gold nanoparticles *via* formation of a thio–gold bond.

4. Electrochemical sensors

Ever since its discovery, graphene has quickly become a material under spotlight for development of new electrochemical sensors because of its unique electrochemical and structural properties.[111] Since graphene has a large electrochemical potential window (approximately 2.5 V in 0.1 mM phosphate buffer saline solution),[112] detection of molecules that have high oxidation or reduction potential (*e.g.*, nucleic acids) become feasible. In addition, edges and defects on graphene provide a high electron transfer rate,[113] suggesting that RGO sheets or small flakes of pristine graphene are superior for electrochemical detection. It has been demonstrated that the electron transfer rate of $Fe^{3+/2+}$ on RGO is more than an order of magnitude higher than that on a glassy carbon electrode (GCE) due to the unique electronic structure of RGO, especially the high density of the electronic states over a wide energy range.[114,115] Electron transfer can be enhanced also because small graphene flakes are able to provide direct electrical wiring between the electrode and the active centers of the redox enzymes.[116] Interestingly, RGO has intrinsic catalytic activity towards some small enzymatic products such as H_2O_2 and NADH, making it attractive for enzyme-based sensors. Owing to its extremely high surface-to-volume ratio (theoretically, 2600 $m^2\ g^{-1}$),[117] graphene based electrodes provide a large effective reaction area and high capacity for enzyme loading. A high surface-to-volume ratio also makes it ideal for functional composite, in which, a small percentage of graphene is able to provide percolating pathways for charge conduction.

Most graphene based electrochemical sensors use RGO because (1) its abundant defects and chemical groups facilitate charge transfer and thus ensure high electrochemical activity; (2) the populated chemical moieties on the RGO surface offer the convenience and flexibility for various functionalizations to enhance the sensor performance; (3) the chemical and electrical properties of RGO are highly tunable; and (4) as compared to non-conductive GO, RGO can efficiently transport charges.

4.1 Detecting hydrogen peroxide

Hydrogen peroxide (H_2O_2) is an enzymatic product of many biological processes. Therefore, detection of H_2O_2 is of great importance. Xu *et al.* fabricated a H_2O_2 sensor using a RGO–chitosan composite film entrapped with hemoglobin (Hb) molecules (Fig. 2a).[118] It exhibits a lower limit of detection (LOD) (0.51 μM) and a wider linear range (6.5–230 μM) as compared with the conventional H_2O_2 detection methods. This is because the RGO–chitosan matrix can be abundantly loaded with Hb molecules and provide a biocompatible microenvironment to retain the enzyme in its native structure. Furthermore, RGO facilitates the electron transfer between the matrix and the electroactive center of hemoglobin and the percolating 3D network of RGOs provide multiplexed paths to rapidly conduct away the charges. In another H_2O_2 sensor, horseradish peroxidase (HRP) was used instead to hydrolyze H_2O_2; and small graphene sheets non-covalently exfoliated by

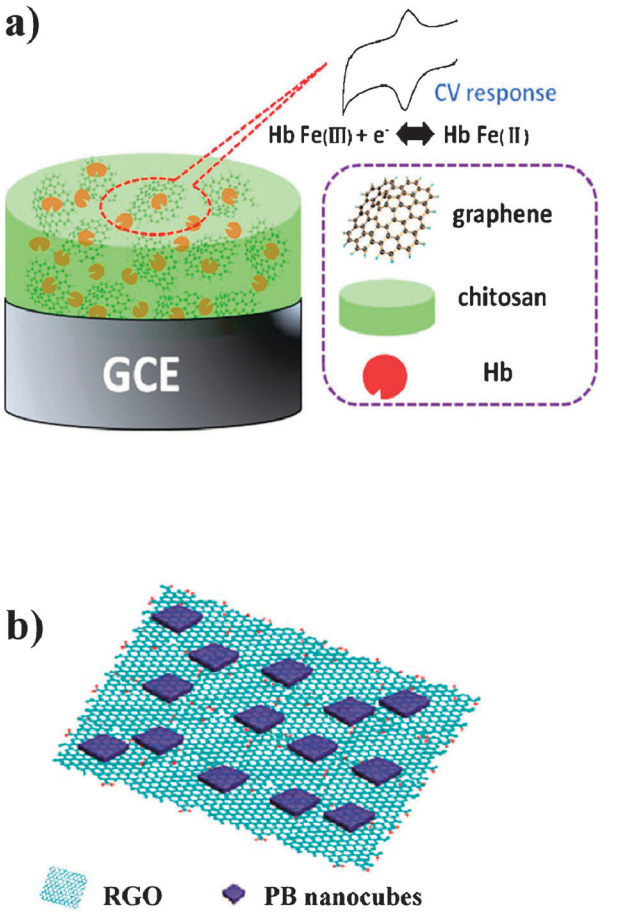

Fig. 2 Graphene-material based electrochemical sensor for detection of H_2O_2. (a) Schematic of the construction of Hb-graphene–chitosan/GCE. Hb = hemoglobin; GCE = glassy carbon electrode; graphene here is actually RGO. Adapted with permission from ref. 118. Copyright 2010 Elsevier B.V. (b) Illustration of a RGO sheet decorated with Prussian blue (PB) nanocubes. Adapted with permission from ref. 129. Copyright 2010 American Chemical Society.

the aromatic molecules (tetrasodium 1,3,6,8-pyrenetetrasulfonic acid) were used to anchor the enzymes with large capacity and to efficiently mediate the charge transfer.[119] This sensor gives a detection limit of 0.106 μM and a linear range from 0.63 μM to 16.8 μM. A novel hierarchical nanostructure formed by layer-by-layer assembly of HRP and sodium dodecyl benzene sulfonate (SDBS) functionalized RGO has been reported by Zeng *et al.* for H_2O_2 detection.[120] An impressively low detection limit (0.1 μM) was achieved due to the high enzyme loading and the fact that enzymes intercalated in RGOs retain high catalytic efficiency towards H_2O_2 with low diffusion barrier. Single-stranded DNAs (ssDNA) which can interact with graphene or RGO through π–π stacking have been utilized to assist material dispersion, to electrostatically attract reactants, or to enhance the loading of enzymes.[121,122]

Electrochemical detection of H_2O_2 can also be catalyzed by metal nanoparticles. Using one-step microwave-assisted thermal reduction, Wang and co-workers have fabricated a platinum nanoparticle/RGO hybrid for H_2O_2 detection.[123] The detection limit of this sensor (80 nM) is several orders lower than other carbon-based electrodes, such as the CNTs/chitosan modified

electrode (10.3 μM),[124] the highly ordered mesoporous carbon modified electrode (1.61 μM),[125] CNTs/silica/Au/Pt hybrid nanomaterial (0.5 μM).[126] And a broad range of linear response is achieved (1 μM–500 μM). The high performance of this sensor can be attributed to the facts that platinum nanoparticles can be uniformly deposited on RGO nanosheets with high density, and rapid charge transfer is ensured by the intimate interaction between metal nanoparticles and RGO and their highly conductive nature. The same group also demonstrated a similar sensor based on a gold nanoparticle/RGO hybrid.[127] Zhou *et al.* incorporated RGO with both nanoparticles (gold) and enzymes (microperoxidase-11), in which gold nanoparticles not only act as the catalyst but also act synergistically with RGO sheets to facilitate charge transfer.[128] The highest sensitivity (45 nM) in all H_2O_2 sensors is realized by decorating the RGO thin-film with *in situ* grown Prussian blue which is a superior electrocatalyst (artificial peroxidase) for H_2O_2 reduction (Fig. 2b).[129]

4.2 Detecting glucose

Glucose detection is clinically significant for diagnosis and management of diabetes. Its electrochemical detection can be realized by using glucose oxidase (GOD) as the mediator or recognition element. A conducting porous matrix, which gives large effective detection surface and high enzyme loading capacity, can be made by mixing RGO with supporting polymers. Kang and co-workers reported a GOD–RGO–chitosan modified electrode that exhibited a wider linear range (from 0.08 mM to 12 mM), a lower LOD (0.02 mM), and a higher sensitivity (37.93 μA mM^{-1} cm^{-2}), as compared with the sensors using other nanostructured materials.[130] The electron-transfer-rate constant (2.83 ± 0.18 s^{-1}) of this sensor is higher than that of multi-walled carbon nanotubes (MWCNTs) based sensors.[131,132] Without using chitosan that may hinder electron transfer, a simple electrode with GOD adsorbed on RGO thin film was fabricated.[133] It offers a LOD of 0.01 mM and sensitivity of 110.0 μA mM^{-1} cm^{-2}. Alwarappan *et al.* constructed a porous matrix with GOD, RGO, and polypyrrole (ppy). The ppy provides excellent conductivity, support to the matrix, and biocompatibility. A ultra-low LOD (3 μM) was reached.[134] A layer-by-layer (LbL) assembly of alternating RGO films and poly(ethyleneimine) (PEI) films with controllable film thickness, morphology, and composition has also been presented.[135] Both glucose oxidase and glucoamylase were loaded into such LbL film to enable simultaneous detection of glucose and maltose, demonstrating the possibility of integrating RGO and multi-enzyme systems in a single multilayer film.

Various strategies have been developed to modify RGO. For instance, ionic liquids have been used to hybridize with RGO.[136,137] Ionic liquids assist to disperse RGO for thin-film fabrication, and can serve as excellent binders between electrolyte and electrode because of their ability to promote electron transfer and ion exchange, their electrochemical stability and biocompatibility. Au nanoparticles have been used to decorate RGO by *in situ* reduction or physical adsorption to improve LOD, detection range, and stability.[112,138] Similarly, platinum nanoparticles have been electrochemically deposited on RGO and an outstanding LOD of 0.6 μM has been achieved for glucose detection.[110] RGO can also be modified by doping. The nitrogen-doped (N-doped) RGO film that possesses a large amount of positive charges can improve the electrochemical detection by enhancing adsorption of O_2, H_2O_2 and other intermediates.[139] Wang *et al.* developed a novel sensor based on a N-doped RGO/Chitosan/GOD/GCE hybrid.[140] It has a detection limit as low as 10 μM. The reduction potential of the electrode was shifted by 400 mV towards positive potential as compared with a bare GCE, indicating its fast electron transfer kinetics.

4.3 Detecting nucleic acids

Graphene materials have also been employed for sensitive and selective electrochemical detection of nucleobases, nucleotides, single stranded DNAs (ssDNA), and double stranded DNAs (dsDNA). Such electrochemical DNA sensors may provide a simple alternative approach for DNA analysis and sequencing.

The four distinct nucleobases (A: adenine, T: thymine, C: cytosine, G: guanine) can be electrochemically differentiated because they have different oxidation potentials. Huang *et al.* used RGO with abundant –COOH groups to electrochemically detect guanine and adenine with a LOD of 50 nM and 25 nM, respectively.[141] The high sensitivity can be ascribed to the excellent electrochemical properties of RGO, the electrostatic attraction between the negatively charged –COOH groups and the positively charged nucleobases, and the strong π–π stacking interaction between the nucleobases and honeycomb carbon lattice. A Fe_3O_4 nanoparticle doped RGO–chitosan electrode has been used to detect guanosine.[142] It was suggested that Fe_3O_4 nanoparticles help to reduce the electron transfer resistance.

Du and co-workers fabricated a RGO electrode decorated with AuNPs by potentiostatic electrodeposition to detect ssDNA.[143] The incorporation of AuNPs was proven to be essential to separate the oxidation signal of T from that of A. And they demonstrated that the electrochemically reduced RGO showed enhanced electrochemical and electrocatalytic activity as compared to chemically reduced RGO. This DNA sensor is able to detect single-base alteration (mutation) without any labeling or probe DNA. Stacked graphene nanofibers (SGNFs) were used by Ambrosi and Pumera to distinguish the four nucleobases with a sensitivity two to four folds higher than carbon nanotube-based electrodes (Fig. 3).[144] The high sensitivity is due to numerous open edges of individual graphene nanosheets which are much more electrochemically active compared to the basal carbon plane. This sensor was employed to examine the base composition of human influenza A(H1N1) DNA strand. In the work of Lim *et al.*, graphene epitaxially grown on SiC was used to detect dsDNA.[145] It was shown that dsDNA can be differentiated from ssDNA, because dsDNA exhibits lower oxidation peaks for A and C and increased oxidation potential for C. Electrochemical detection of dsDNA is not possible with the conventional electrodes (*e.g.*, gold electrode and GCE) due to their limited electrochemical potential window. The authors also demonstrated that electrochemical anodization to introduce oxygenated groups onto graphene largely improved the electrode performance.

A GO modified electrode was used for detection of DNA hybridization.[146] In this work, probe ssDNA molecules that lack guanine base were covalently immobilized onto a GO film,

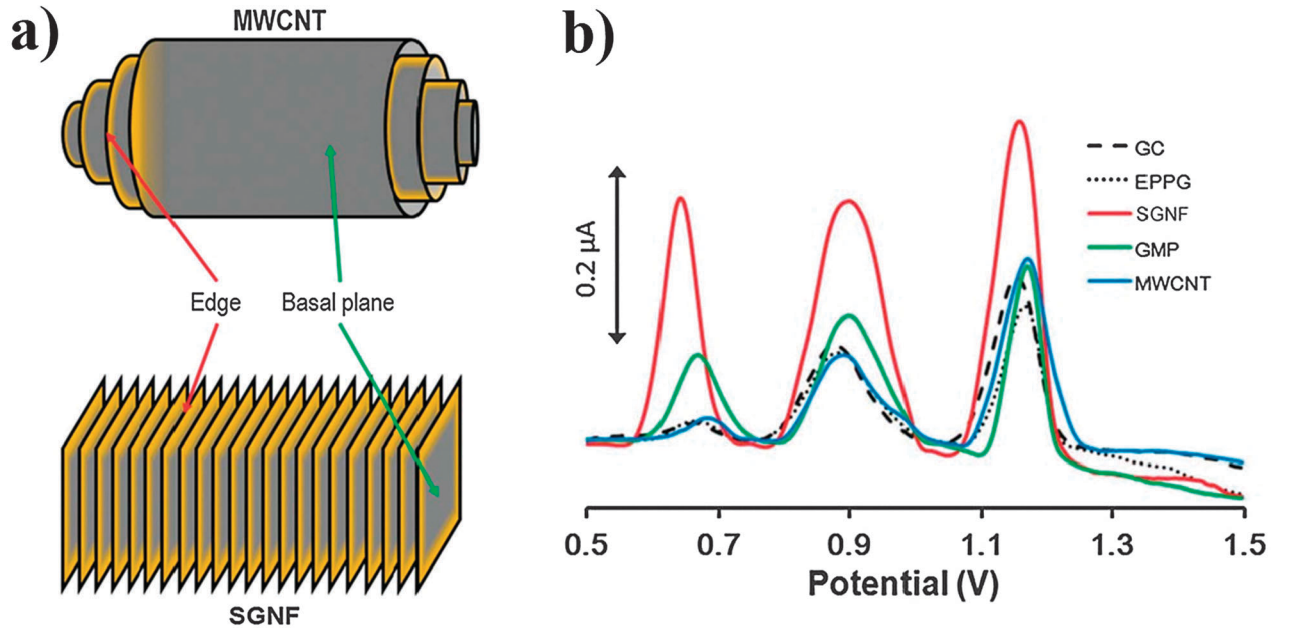

Fig. 3 Graphene-based electrochemical DNA sensor. (a) Schematics of graphene sheet orientation in multiwalled carbon nanotubes (upper) and stacked graphene nanofibers (lower). The highly electroactive edge portion of the sheets is represented in yellow. (b) Differential pulse voltammetry (DPV) for ssDNA of the human influenza A(H1N1) obtained from SGNF (stacked graphene nanofibers, red), GMP (graphite microparticle, green), MWCNT (multi-walled carbon nanotubes, blue), GC (glassy carbon, black dashed), and EPPG (edge plane pyrolytic graphite, black dotted) electrodes. Adapted with permission from ref. 144. Copyright 2010 the Owner Societies.

and hybridization was detected by the guanine oxidation signal from the target ssDNA molecules (a hepatitis B virus specific sequence). In an interesting demonstration by Zhao *et al.*, RGO quantum dots ($\sim$10 nm) were used to modify the pyrolytic graphite electrode for detection of DNA hybridization.[147] When the target ssDNA hybridizes with the pre-immobilized probe ssDNA, the electron transfer from the electrochemically active species $[Fe(CN)_6]^{3-/4-}$ was increased because the blocking effect by the probe ssDNA was alleviated. A LOD of 100 nM was reached. This study suggests the potentials of RGO quantum dots in electrochemical sensing. The good performance of RGO quantum dots may be attributed to their abundant edge sites (electrochemically active sites) and quantum confinement effects. Based on a similar sensing scheme, Wang *et al.* showed a RGO based sensor to detect hybridization of methicillin-resistant *Staphylococcus aureus* DNA with a LOD of 100 fM.[148] However, the authors proposed an opposite mechanism. They argued that hybridized DNAs remained on the RGO surface and caused an increase of electron transfer resistance (hence a decrease in the electrochemical signal). The discrepancy between Zhao's work and Wang's work may be because of the size difference between RGO quantum dots and RGO sheets. Larger RGO sheets likely can bind more strongly with hybridized DNAs.

Hypoxanthine is a purine derivative. A hypoxanthine sensor was constructed using an electrode consisting of RGO, conducting polypyrrole graft copolymer, poly(styrenesulfonic acid-*g*-pyrrole), and enzyme xanthine oxidase.[149] The detection mechanism of such a sensor involved two-steps of oxidation: oxidation of hypoxanthine catalysed by xanthine oxidase, and subsequent oxidation of uric acid and H_2O_2 produced from the previous reaction. RGO and the conducting polymer interact with π–π stacking and form a nanocomposite with high conductivity and an excellent electrocatalytic environment. As a result, a LOD of 10 nM was obtained. As hypoxanthine accumulates continuously from adenine nucleotide degradation after fish death, this sensor was employed to assess fish freshness.

4.4 Detecting protein markers

Graphene based electrochemical sensors have also been developed to detect various protein biomarkers. Su *et al.* fabricated a label-free immunosensor to specifically detect cancer marker alpha fetoprotein (AFP) using layer-by-layer construction with electropolymerized thionine (TH) film, GO–chitosan composite, AuNPs, and conjugates of horseradish peroxidase (HRP) and anti-AFP antibody.[150] Binding of AFP molecules to the antibodies partially blocks the active center of HRP and consequently decreases the catalytic reduction of H_2O_2 by HRP (thus a decrease in the electrochemical signal). The electroactive TH acts synergistically with HRP to mediate the electron transfer from H_2O_2 to the electrode. The achieved LOD (0.7 ng ml^{-1}) is much better than the conventional enzyme-linked immunosorbent assays (ELISA). This sensor was challenged with clinical human serum samples and the negative/positive samples were correctly identified in accordance with the results from a commercial clinical device. A simpler AFP sensor was made by incorporating TH with RGO film through π–π interaction followed by covalent crosslinking of AFP antibodies with TH.[151] Binding of AFP molecules blocks the electron-transfer and mass-transfer, leading to a decrease of electrochemical signal originated from the redox reactions of TH. In comparison with other sensors, such as carbon nanotube or nanoparticle derived AFP sensors, a much lower LOD (5.77 pg ml^{-1}) was achieved, due to the high

electron transfer rate between the intimately interacted RGO and TH, and high loading of TH molecules and AFP-antibodies because of the large surface area provided by the RGO film. The sensor was successfully used to determine AFP in serum samples.

Du *et al.* used a different strategy to detect AFP.[152] In their work, AFP molecules bound to the primary-antibody-functionalized RGO electrode complex again with carbon nanospheres (CNS) tagged with the secondary antibodies and HRP molecules, leading to an increased electrochemical signal from redox reaction of H_2O_2. The use of RGO and CNS gave a 7-fold increase in the detection sensitivity, because of the superior electrochemical and electrical properties of RGO and the ability of CNS to carry multiple HRP molecules. A 20 pg ml^{-1} LOD was demonstrated. A similar sensor to detect prostate-specific antigen (PSA) (marker for prostate cancer) based on sandwich immunoreactions on top of RGO modified electrode has been reported (Fig. 4).[153] In comparison with Du's work, CNS were replaced by small RGO flakes, because RGO flakes can carry more secondary antibodies and more HRP molecules due to their extremely large surface-to-volume ratio. Here, dual functionalities of RGO were utilized, *i.e.*, firstly as the electrode material and secondly as the enzyme carrier. An impressive detection limit of 1 pg ml^{-1} was demonstrated, superior to other PSA sensors including a sensor using carbon nanotube–HRP conjugates.[154] A sandwich-like immunodetection of carcinoembryonic antigen (CEA) which is a marker for colorectal cancer was developed by Zhong *et al.*[117] In their work, a nanocomposite of gold nanoparticles (AuNPs), RGO and chitosan was used to carry multi-copies of the HRP-conjugated CEA-specific secondary antibody onto a glassy carbon electrode modified with Prussian blue and AuNP. 10 pg ml^{-1} CEA can be detected. In another demonstration, a RGO modified electrode for sandwich-like immunodetection of immunoglobulin G (IgG) in human serum was developed.[155]

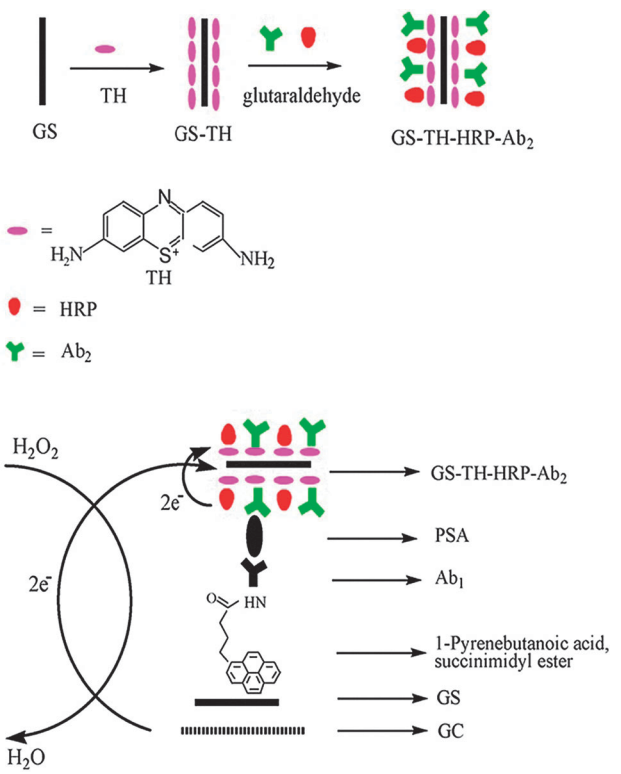

Fig. 4 Schematic illustration of an electrochemical immunosensor for detection of prostate specific antigen (PSA). GS = reduced graphene oxide sheet; TH = thionine; HRP = horseradish peroxidase; Ab2 = secondary anti-PSA antibody; Ab1 = primary anti-PSA antibody; GC = glassy carbon electrode. Adapted with permission from ref. 153. Copyright 2010 Elsevier B.V.

4.5 Detecting other biomolecules

Dopamine (DA) is an important neurotransmitter, deficiency of which underlies Parkinson's diseases. DA detection is challenged by its low physiological concentration (0.01 μM–1 μM) and interference from much more abundant ascorbic acid (AA) and uric acid (UA). A chitosan–RGO composite electrode for DA detection was demonstrated by Wang *et al.*[156] A linear detection range (5–200 μM) was achieved in the presence of a large excess of AA or UA (500 μM). In addition, they showed that the chitosan–RGO electrode outperformed the electrode made of chitosan and multi-walled carbon nanotubes. Hou *et al.* demonstrated an electrochemical sensor to selectively detect dopamine with a LOD of 0.01 μM based on a composite electrode made of Nafion and *N*-(trimethoxysilylpropyl) ethylenediamine triacetic acid (EDTA) modified RGO.[101] The high performance arises from several reasons: (1) dopamine can interact with RGO *via* π–π interaction; (2) EDTA groups, combined with ionic sulfuric groups of Nafion, can concentrate DA from the solution; (3) EDTA groups linked to the RGO surface promote electron transfer as evidenced by the narrower potential separation between the anodic and cathodic peaks (ΔE_p); (4) the oxygen containing functional groups on RGO block the diffusion of AA and thus eliminate its interference. In another work, detection of DA at 5 nM was realized in the presence of excess AA using a β-cyclodextrin/RGO nanocomposite electrode.[157] β-Cyclodextrin functionalization assists dispersion of RGO sheets, and greatly improves the electrochemical performance. As compared with the bare RGO electrodes, the β-cyclodextrin/RGO electrodes exhibited a two-orders-of-magnitude-lower LOD, attributable, at least in part, to the faster electron transfer rate (ΔE_p was reduced from 115 mV to 73 mV).

AA and UA sensors have also been developed using graphene materials. For example, Keeley *et al.* demonstrated an AA sensor using graphene nano-sheets exfoliated in liquid by dimethylformamide (DMF).[65] A UA sensor was constructed by self-assembling gold nanoparticles (AuNPs) onto pyrene-butyrate functionalized RGO (PFG) sheets.[158] A LOD of 0.2 μM was obtained. Shang *et al.* utilized a novel microwave plasma enhanced CVD method to obtain multilayer graphene nanoflake films (MGNFs) vertically grown on a silicon substrate.[159] DA, AA, and UA can be unambiguously distinguished by three well-defined peaks that appeared in the cyclic voltammogram (CV). Furthermore, near-ideal electron transfer kinetics was evidenced by the narrow ΔE_p (61.5 mV at the scan rate of 10 mV s^{-1}) which is close to the ideal value of 59 mV. Such a fast electron transfer process is due to the abundant edge planes and defects on the nanoflakes, unique

electronic structure of graphene, and the good electrical contact between MGNFs and silicon substrate.

Cholesterol is an essential constituent of cell membranes.[160] However, undesired accumulation of cholesterol and its esters causes critical health problems, such as heart diseases, cerebral thrombosis, and atherosclerosis. A sensitive amperometric sensor based on functionalized RGO sheets has been developed for detection of cholesterol and its esters with a LOD of 0.2 μM.[161] Cholesterol esterases and cholesterol oxidases were loaded onto the electrode to catalyze the hydrolysis of cholesterol and its esters, and consequently, generate H_2O_2. Platinum nanoparticles decorated on RGO sheets, in turn, catalyze the electrochemical oxidization of H_2O_2. Nafion coating was used at the same time to block other irrelevant analytes (*e.g.*, ascorbate and urate).

4.6 Cellular detection

Detecting rare pathological cells is of obvious clinical significance. Feng and co-workers fabricated a sensitive and selective RGO-based electrochemical biosensor to detect cancer cells with overexpressed nucleolin on plasma membrane (*e.g.* breast cancer cells and human cervical carcinoma cells), at a LOD of thousand cells per ml.[162] To avoid RGO aggregation and introduce more –COOH groups, 3,4,9,10-perylene tetracarboxylic acid (PTCA) was used to composite with RGO. And the nanocomposite was covalently functionalized with NH_2-modified nucleolin-specific aptamers (oligonucleotides serving as highly selective antibodies) as the recognition element. The binding of cancer cells increases the electron transfer resistance by blocking the access of the redox probe ($[Fe(CN)_6]^{3-/4-}$).

Electrochemical detection in amperometry mode provides high temporal resolution (milliseconds). Therefore, it is suitable to detect dynamic cellular activities in real-time. A RGO based sensor for detection of the real-time kinetics of oxygen release from human erythrocytes in response to $NaNO_2$ stimulation has been shown.[163] Two kinds of excellent mediators for O_2 reduction, namely, laccase (Lac) and 2,2-azino-bis(3-ethylbenzothiazoline-6-sulfonic acid) (ABTS), were functionalized onto RGO sheets to form a Lac–ABTS–RGO hybrid electrode. An O_2 level as low as 10 μM can be detected by this hybrid electrode.

Cellular release of reactive oxygen species (such as H_2O_2) is an early indicator for cytotoxic events and cellular disorders. A RGO based electrochemical sensor has been coupled with live human breast cancer cells (MCF-7) to detect triggered cellular release of H_2O_2 in real-time and with a LOD of 0.1 μM.[164] To construct the electrode, RGO sheets were first electrophoretically deposited on the indium tin oxide (ITO) glass. This was followed by electrodeposition of Prussian blue (artificial H_2O_2 catalyst) and adsorption of extracellular matrix proteins (laminin) to promote cell adhesion. Ten layers of RGO–PB–laminin were formed on the ITO substrate using layer-by-layer deposition. *In situ*, real-time, sensitive, and quantitative detection of extracellular H_2O_2 release from live cells was demonstrated. Specifically, it was determined that, upon stimulation of phorbol-12-myristate-13-acetate (PMA, 5 μg ml^{-1}), 10^{11} H_2O_2 molecules were released from a single MCF-7 cell over 25 s.

4.7 Detecting other chemicals

Graphene based electrochemical sensors have also been employed to detect environmental contaminants (paraoxon,[165] nitromethane,[166] heavy metal ions,[167–169] hydroquinone and catechol,[170] methyl jasmonate,[171] hydrazine[172]), pharmaceutical compounds (paracetamol,[173] 4-aminophenol,[174] aloe-emodin,[175] Rutin,[176] *etc.*), industrial compounds (ethanol[177]), and explosives (TNT[178]).

5. Electronic sensors

Nanoelectronic sensing based on one-dimensional (1D) semiconducting nanomaterials (*e.g.*, carbon nanotubes, silicon nanowires) is an emerging sensing modality that offers high sensitivity, high temporal resolution, simple label-free detection scheme, and suitability for development of lab-on-a-chip devices.[14,22,28] Silicon nanowire (SiNW) is perhaps the mostly explored 1D material for nanoelectronic sensing with great successes.[23,179–181] However, a major limitation of SiNW sensors is that their detection relies essentially on the induced field-effect. Therefore, they are only suitable to the detection of charged analytes or electrogenic events. Two-dimensional graphene has been added as a new building block for nanoelectronic sensors, taking advantages of its extraordinary electrical properties. It provides vast new possibilities.

Graphene exhibits remarkably high carrier mobility, high carrier density, and low intrinsic noises. These characteristics promise a high signal-to-noise ratio in detection. And the conductance of graphene is highly sensitive to the local electrical and chemical perturbations because every atom of a graphene film is exposed to the environment. In addition, the Fermi level of zero-bandgap graphene can be modulated by the gate voltage, therefore, the charge carriers can be either holes or electrons depending on the gate voltage. Such ambipolar property allows readily setting the desired working point. When detection is based on the field-effect, a large bandgap is desired. The bandgap of graphene can be opened by reducing its dimension(s) to nanoscale[182,183] or by introducing atomistic or chemical dopants.[63,184,185] Moreover, as compared to 1D nanostructured sensing elements, the 2D structure of graphene can provide a larger detection area, and homogeneous surface for uniform and effective functionalization. And it is more suitable to intimately interface with flat cell membranes. It has been shown that graphene is able to support cell adhesion and growth, indicating its biocompatibility.[186,187] In addition, the outstanding optical transparency of graphene allows simultaneous electrical measurement and optical observation. The ballistic transport property of graphene, however, deteriorates to some extent in RGO due to its defective nature. On the other hand, as discussed earlier, RGO offers rich chemistry for functionalization; can be obtained through facile, scalable and low-cost syntheses; enables solution-based fabrication; and possesses tunable electrical properties.

5.1 Detection mechanisms

Graphene electronic sensors are usually referred to as field-effect transistors (FETs) because, similar to the conventional FETs, graphene conductance can be sensitively modulated by minute gating signals. This, however, is somewhat misleading

because it implies that the detection is achieved only through the field-effect introduced by the sensing targets. But actually, graphene-based electronic detection can be realized through other mechanisms as well, such as doping effects, charge carrier scattering, change of local dielectric environment. Therefore, graphene nanoelectronic sensors provide a versatile platform for a wide spectrum of sensing purposes.

In solution, a thin ionic double-layer or Debye layer (<1 nm in thickness at physiological ionic strength) forms on top of graphene, which creates a large double-layer capacitance (C_{dl}). C_{dl} is much larger than the capacitance of the dielectric gate layer (typically >100 nm in thickness) in back-gated graphene FETs. Therefore, the transconductance (the ratio of drain-source current change over gate voltage change) of liquid-gated graphene FETs is >100 times larger than that of back-gated FETs.[188,189] Although the overall field-effect of graphene is not prominent, significant current response of graphene to minute field-effect induced by charged molecules or cellular electrical activities is guaranteed by the enhanced transconductance in solution as well as the high conductivity and low noise of graphene.

Graphene electronic sensors can also utilize the doping effects (direct charge transfer between the absorbed analytes and the graphene) because the zerogap electronic structure of graphene is amenable to charge transfer, even with molecules that have a small chemical-potential mismatch. Many molecules, particularly, those possessing aromatic rings, can intimately interact with graphene. Such strong interactions strengthen the doping effect and consequently allow sensitive electronic detection. It has been suggested that open-shell adsorbates can directly transfer charges to or from graphene, causing strong doping effects.[190] Close-shell adsorbates are not able to directly transfer charge with graphene. But they may produce 'indirect doping' by altering the charge distribution within graphene or influencing the existed doping from the supporting substrate or 'impurities' on graphene. Another form of 'indirect doping' is electrochemical doping while charge-donating redox reactions occur at the graphene surface.[191] When Gibbs free energy of the reaction plus the energy required for electron transfer is negative, redox reaction and charge transfer occur spontaneously on the graphene surface.

Alterations of the local dielectric environment may underlie the graphene device response too. For example, binding of biomolecules could alter the local dielectric constant or local ionic strength, which, in turn, modulates C_{dl} and thus carrier density in graphene.[189,192] Such dielectric changes could also affect the screening of impurity on graphene surface or long-range electrostatic interaction between the graphene and the substrate, resulting in measurable change in the transport current.[189]

The scattering effect is another sensing mechanism that can be exploited. Adsorbates may cause scattering of electrons or holes, and consequently decrease carrier mobility thus conductance of graphene.[38] Oppositely, adsorbates may alleviate the scattering effect caused by the supporting substrate, leading to an increase in graphene conductance.[193,194] Furthermore, detection may arise from pH change,[105] expansion or deformation of the graphene lattice,[195–197] or the modulation of the Schottky energy barrier between the graphene film and the metal electrodes or between the individual flakes in a graphene network.[198] In some cases, detection is determined by a dominant mechanism while, in other cases, it results from the combination of several mechanisms. Therefore, scrutiny is required to interpret the sensor response.

5.2 Detecting gases

The very first graphene sensor is actually an electronic one for gas detection, demonstrated by Novoselov and co-workers (Fig. 5).[38] It used mechanically-exfoliated few-layer pristine graphene as the sensing element and was applied to detect NO_2 gas (an open shell molecule). By measuring the change of source–drain resistance, 1 ppb NO_2 can be detected. Strikingly, by monitoring the change of the Hall resistance, adsorption or desorption of single NO_2 molecule can be clearly resolved as a step-like signal originated from transfer of single electron. This ultimate sensitivity achieved at room temperature is due to that graphene conductance is extremely responsive to the minute environmental perturbation, and also because of the extremely low intrinsic noise of nearly-defect-free graphene. Few-layer (3–5 layers) graphene sheets were most electrically quiet because of their low contact resistance with the metal electrodes. The authors also demonstrated that graphene ~ 1 μm in size provided the optimal signal-to-noise ratio. Smaller devices exhibited higher $1/f$ noise because defects at the edges become more prominent, while larger devices gave smaller relative change of resistance. This remarkable study has stimulated tremendous enthusiasm to develop graphene electronic sensors.

Various gas sensors based on graphene materials have been demonstrated thereafter.[198–202] For example, a NO_2 sensor was fabricated by placing a RGO micro-sheet between two Au electrodes.[198] Electron transfer from RGO to adsorbed NO_2 molecules caused hole enrichment in the p-type RGO sheet and consequently increased its conductance. To accelerate the sensor recovery, low-temperature heating and UV illumination were used to de-adsorb the gas molecules. Commonly, graphene devices are made on Si/SiO_2 substrates. Nomani *et al.* demonstrated that 6H-SiC substrates are better than the conventional Si/SiO_2 substrates because the interaction between C-face of SiC and graphene leads to less scattering events (thus higher conductivity and lower noise).[203] As a result, graphene sensors fabricated on the 6H-SiC substrate can detect NO_2 at a lower concentration (10 ppb)[203] as compared to the graphene sensors made on Si/SiO_2 substrates.[204] Jeong *et al.* developed a flexible NO_2 gas sensor by growing a vertically aligned carbon nanotube array on an RGO thin-film network using plasma enhanced CVD to form a nanocarbon hybrid on a polyimide substrate.[199] A stable performance can be maintained even under extreme bending owing to the excellent mechanical flexibility of RGO film. Another flexible NO_2 sensor was demonstrated by Dua *et al.* which provides a ultralow LOD (~ 400 ppt).[201] The RGO thin-film network was inkjet-printed on a poly-(ethylene terephthalate) (PET) plastic film. The authors attributed the high sensitivity to two reasons: (1) the mild reduction agent used (ascorbic acid) introduces less defects as compared with the common agent (hydrazine); (2) the RGO film is highly uniform due to the controllable inkjet-printing process on the PET substrate.

Dinitrotoluene (DNT), a highly volatile chemical, is often detected as a reporter of explosive trinitrotoluene (TNT).

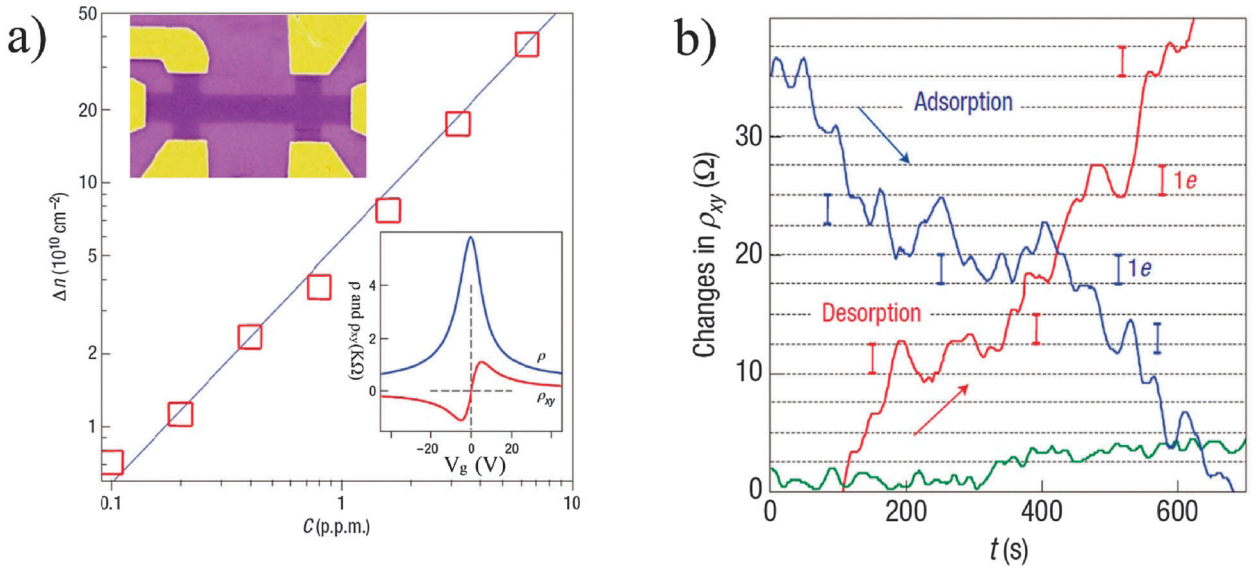

Fig. 5 Electronic detection of individual gas molecules adsorbed on mechanical exfoliated single-layer graphene. (a) Concentration (Δn) of chemically induced charge carriers in graphene exposed to different concentrations (C) of NO_2. Upper inset: scanning electron micrograph of this device. Lower inset: characterization of the graphene device by using the electric-field effect. (b) Examples of changes in Hall resistivity of a three-layer device observed near the neutrality point during adsorption of strongly diluted NO_2 (blue curve) and its desorption in vacuum at 50 °C (red curve). The green curve is a reference—the same device thoroughly annealed and then exposed to pure He. To measure Hall resistivity, ρ_{xy}, $B = 10$ T was applied perpendicular to graphene's surface. The curves are for a three-layer device at $B = 10$ T. The grid lines correspond to changes in ρ_{xy} caused by adding one electron charge, $e(\delta R \approx 2.5\ \Omega)$, as calibrated in independent measurements by varying V_g. For the blue curve, the device was exposed to 1 ppm of NO_2 leaking at a rate of $\sim 10^{-3}$ mbar l s^{-1}. Adapted with permission from ref. 38. Copyright 2007 Nature Publish Group.

A DNT sensor was realized using a spin-coated RGO thin-film.[202] Similar to NO_2, DNT is a *p*-type dopant with strong electron-withdrawing ability. A detection limit of 28 ppb was obtained, which is much lower than the vapour pressure (173 ppb) of DNT at 298 K. A similar RGO sensor constructed by Robinson *et al.* showed a markedly improved LOD (0.1 ppb) for DNT detection.[205] The authors also showed that such RGO sensors are superior to single-walled carbon nanotube (SWCNT) sensors largely due to the much reduced low-frequency ($1/f$) noise.

Although close-shelled gas molecules are weak dopants, graphene sensors targeting on these gases have also been devised. For instance, a H_2 sensor using RGO thin-film was reported by Shafiei *et al.*[206] SiC was employed as the substrate partly because of the high breakdown voltage of the insulating SiC. A platinum (Pt) layer was deposited on top of the RGO film, serving as the catalyst to breakdown H_2 molecules. The dissociated hydrogen atoms diffuse into the interface between RGO and Pt and lower the energy barrier between the two materials, thereby promoting the electron transfer from RGO to Pt. As the result, conductance of RGO film is increased due to the increased hole density. It has been suggested that RGO obtained by mild thermal reduction (at 300 °C; with final oxygen content of 11.39% on RGO) gives the best sensitivity to H_2 due to the optimal trade-off between the conductivity and the density of defect sites for molecular adsorption and catalysis.[207] Johnson *et al.* used palladium (Pd)-coated multi-layer graphene nano-ribbon (GNR) networks for H_2 detection.[208] High sensitivity ($\sim$55% percentage change of resistance to 40 ppm H_2 at room temperature) and good repeatability were achieved.

Massera *et al.* demonstrated a RGO based humidity sensor whose conductance increase is proportional to the H_2O increments in the gas carrier.[209] However, such change is not sustainable due to quick de-adsorption of water molecules. This problem is solved by another group using a thin-film matrix of RGO and polyvinylpyrrolidone nanosphere which is able to stably trap water molecules inside.[210] The increase of RGO conductance is because the adsorbed water molecules shift the substrate's impurity bands and hence their hybridization with the bands of RGO.

A RGO sensor was developed for detection of a poison gas H_2S, with the detection limit of 2 ppm at room temperature.[211] The sensor was fabricated by growing zinc oxide nanorods (ZnO NRs) on RGO. The detection is resulted through two step reactions. Firstly, ambient O_2 molecules adsorbed on ZnO NRs are converted into oxygen ionic species, causing a strong p-doping effect on RGO. Such p-doping is then alleviated by H_2S molecules which react with those oxygen ionic species, leading to a conductance increase of the n-type operated RGO.

Lu *et al.* fabricated a RGO sensor to detect NH_3 under ambient conditions.[212] The authors demonstrated that RGO operated in n-type mode by applying a sufficiently positive gate voltage (V_g) gave better performance (*i.e.*, faster response and faster recovery) than biased at p-type mode. The difference could be attributed to the ambipolar transport of RGO and V_g-induced effects, such as the change in the graphene work function and the Coulomb interaction between NH_3 and graphene. In an interesting work by Yu *et al.*, an electronic NH_3 sensor was developed using vertically oriented graphene sheets obtained from plasma-enhanced chemical vapor deposition (PECVD).[213] The authors suggested that such carbon nanowall structure provides a large surface area for sensitive detection.

Graphene based electronic sensors have been used to detect other vapours as well, including trimethylamine,[214] HCN,[205] I_2,[38] methane,[215] ethanol.[216] It has been suggested that ssDNA decorated on the graphene surface can significantly improve the sensing performance by concentrating water and the target vapour molecules.[217]

5.3 Chemical detection

A pH sensor using few-layered graphene sheets grown on SiC is the first graphene sensor for detection in solution.[218] By monitoring a shift in the Dirac (neutral) point, this sensor provides an ultra-Nernstian pH sensitivity (98 mV per pH *vs.* 59.2 mV per pH). The authors proposed that the detection mechanism involves pH-dependent surface potential modulation (field-effect) by ion adsorption and the attached amphoteric OH^- groups. Also as suggested by the authors, such high sensitivity is attributable to the high carrier mobility of epitaxial graphene which is an order of magnitude higher than that of hydrogen-terminated diamond or silicon. More recently, Ohno *et al.* investigated pH sensing ability of mechanically exfoliated graphene and found that the detection limit of pH was 0.025, which is more than 26-fold lower than carbon nanotube based electronic pH sensors.[219]

Zhang *et al.* demonstrated a heavy metal sensor using mechanically exfoliated graphene with a detection limit of 10 ppm (~5 μM) for Hg^{2+}.[220] Graphene was modified with self-assembled 1-octadecanethiol whose thiol groups have high binding affinity with heavy metal ions. Recently, Chen and co-workers demonstrated a metal ion sensor based on centimetre-long and micrometre-wide RGO thin-film made by microfluidic patterning.[221] By functionalizing Ca^{2+}-binding proteins (calmodulin) onto RGO, Ca^{2+} at a concentration of 1 μM can be detected. The detection depends on the field-effect induced by the positively charged Ca^{2+} ion. By functionalizing heavy-metal-ion-binding proteins (metallothionein type II protein, MT-II) onto RGO, a trace amount (as low as 1 nM) of heavy metal ions (*e.g.*, Hg^{2+}, Cd^{2+}) can be distinctly detected. The authors proposed that the detection is through the altered field-effect from negatively charged MT-II as it undertakes conformational change upon binding with heavy metal ions. This sensor worked properly with lake water samples which are a complex soup consisting of various ions, microorganisms, and impurities, demonstrating its practical use for environmental monitoring.

Myers *et al.* used octadecylamine (ODA) functionalized RGO nanocomposites as the sensing elements to electrically detect benzene, toluene, ethylbenzene, xylenes and cyclohexane with LOD of ppm.[192] The authors proposed that the adsorption of target molecules increases the electron tunnelling barrier between RGO sheets, leading to a decreased conductance.

5.4 Biomolecular detection

Graphene electronic biosensors have been developed to detect the building blocks of living beings, such as saccharides,[106] proteins,[109,222–224] and DNAs.[99,225] Chen and co-workers fabricated a CVD-grown graphene sensor to electrically detect glucose and glutamate, with a LOD of ~0.1 mM and ~5 μM respectively (Fig. 6a).[106] The detection is mediated by the functionalized enzymes, specifically, glucose oxidase (GOD) and glutamate dehydrogenase (GluD). The catalytic reactions mediated by both enzymes produce H_2O_2, which, being a strong electron withdrawing molecule (p-dopant), can increase the conductance of graphene film operated in the p-type regime. The authors also showed that the graphene sensors outperformed thin-film network devices made of single-walled carbon nanotubes.

Most proteins bear charges or dipoles under physiological conditions. This provides possibilities for electronic detection through the field-effect or scattering effect. And many proteins possess aromatic-ring-containing amino acids on the surface.

Therefore, they can firmly bind to graphene *via* π–π interaction and therefore may be detected through the doping effect. However, due to the complex structure of proteins, the sensor response may be resulted from a single dominant effect (*e.g.*, doping) or be simultaneously influenced by multiple effects depending on the charges, amino acid composition, and orientation of the interacting proteins. So, interpretation of the detection results requires caution. Ohno *et al.* used a pristine graphene device to detect bovine serum albumin (BSA) with a LOD as low as 0.3 nM.[222] Non-specific adsorption of BSA molecules caused conductance increase of graphene biased at the p-type region, due to the field-effect induced by the negatively charged BSA molecules. This sensor, however, lacks specificity in detection.

In an electronic immunoglobulin E (IgE) sensor, to assure specificity, IgE-specific aptamers were functionalized onto the

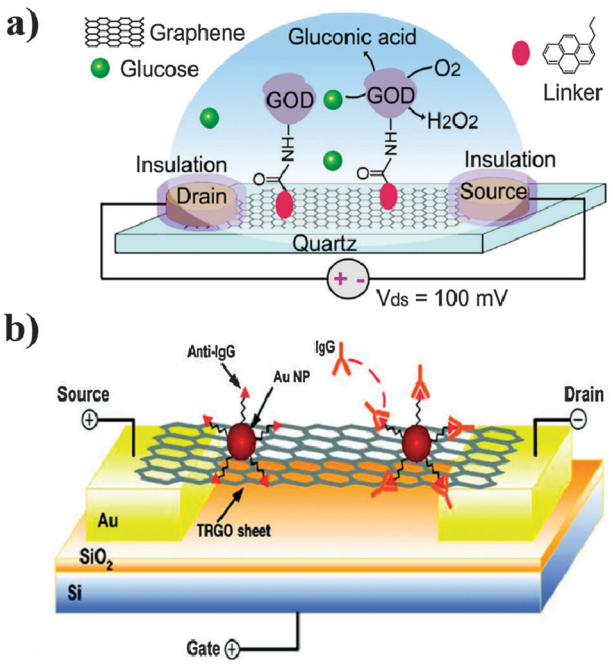

Fig. 6 Electronic graphene sensors for biomolecular detection. (a) Schematic illustration of a glucose oxidase (GOD) functionalized CVD-graphene device for detection of glucose. Adapted with permission from ref. 106. Copyright 2010 the Royal Society of Chemistry. (b) Schematic of a FET device based on a suspended thermally-reduced graphene oxide (TRGO) for detection of immunoglobulin G (IgG). Anti-IgG molecules are anchored to the TRGO sheet through gold nanoparticles (AuNPs). Adapted with permission from ref. 109. Copyright 2010 Wiley-VCH Verlag GmbH & Co. KGaA, Weinheim.

surface of mechanically exfoliated graphene monolayer *via* a linker molecule (1-pyrenebutanoic acid succinimidyl ester).[226] When the positively charged targets (IgE) were introduced, the conductance of p-typed graphene decreased dramatically due to the field effect. Mao *et al*. developed a RGO thin-film based sensor to detect immunoglobulin G (IgG) with an ultralow detection limit of ~13 pM (Fig. 6b).[109] To realize specific detection, AuNPs and anti-IgG antibody conjugates were assembled onto RGO sheets by electrospray and electrostatic force directed assembly. In addition, a blocking buffer (a cocktail solution containing Tween 20, fish gelatin and BSA) was used to passivate unfunctionalized sites on RGO sheets, so that, non-specific binding of irrelevant molecules was minimized. Similarly, Yang and Gong reported an immunosensor for detection of prostate specific antigen (PSA) using RGO sheets exfoliated from graphite by a thermal expansion method. 1-Pyrenebutanoic acid succinimidyl ester (PBSE) was used as the linker molecule for antibody immobilization and BSA was used to block non-specific binding.[224] A wide linear detection range (0.1–100 ng ml^{-1}), which covers the physiological concentration (1–10 ng ml^{-1}) in human serum, was obtained. In addition, the sensor is re-usable after the treatment with glycine–HCl solution to break the antibody–antigen linkage. The authors proposed that conductance decrease after addition of PSA is due to blocking of current transport between percolating RGO sheets by the intercalating non-conductive PSA molecules.

Recently, an all-RGO device (*i.e*., conducting channel and source/drain electrodes were all made of an RGO thin-film network) fabricated on a transparent and flexible substrate was demonstrated by He *et al*. and used as a protein sensor.[55] After the RGO channel being biotinylated and subsequently passivated, this device was used to specifically detect avidin with a LOD of ~80 nM based on the p-doping effect from the binding avidin molecules. It is worth mentioning that this sensor is transparent and bendable. The electrical characteristics of the device did not alter even after 5000 bending cycles owing to the excellent flexibility of the RGO film. In an interesting work reported by Myung *et al*., a chain of RGO-encapsulated SiO_2 nanoparticles (NPs) was used as the conducting (sensing) channel.[227] RGO sheets can self-assemble onto 3-aminopropyltriethoxysilane (APTES) modified SiO_2 NPs (100 nm in diameter). Such 3D nanostructure provides a large surface area for functionalization of recognition elements and thus for detection. By functionalization with specific antibodies, breast cancer biomarkers, human epidermal growth factor receptor 2 (HER2) and epidermal growth factor receptor (EGFR) could be selectively detected with low LOD (100 pM for HER2 and 10 nM for EGFR). Binding of positively charged HER2 or EGFR molecules on the RGO surface induces a positive gating effect which, in turn, reduces the hole density in the p-type RGO (and hence its electrical conductance).

Graphene electronic sensors have also been employed for detection of DNA molecules. Mohanty and Berry demonstrated an electronic DNA sensor using a microsized graphene oxide (GO) sheet.[100] Although being called as 'GO' by the authors, the chemically derived graphene used in this work is conductive, *i.e*., electrically similar to RGO. They functionalized the 'GO' sheets with probe ssDNA *via* simple physical adsorption taking advantage of the firm π–π interaction between DNA bases and 'GO'.[100] Conductance increase of 'GO' was used to indicate the hybridization of the target bacterial ssDNA, as a result of doping effect. It is noted that the electrical measurements were made under dry conditions; therefore, DNA molecules are not charged and thus lack ability to impose the field-effect. The authors determined that hybridization of a pair of target and probe ssDNA produces one sixth quantum of hole doping (p-doping). Another DNA sensor was made alternatively with CVD-grown graphene by Dong *et al*.[225] It was able to detect hybridization of target ssDNA in solution with single-base-mismatch specificity and a LOD of 10 fM. The authors suggested that detection (decrease of graphene conductance) is based on DNA induced n-doping on graphene, instead of the field-effect and impurity screening mechanism. This is different to the p-doping mechanism under dry conditions as proposed by Mohanty and Berry.[100] In addition, Dong and co-workers showed that decoration of gold nanoparticles (AuNPs) can increase the detection range. This is because one AuNP can covalently associate with multiple thiolated probe ssDNA molecules, whereby increases the loading efficiency and capacity. Similar to the results obtained by Dong *et al*., another team of researchers also observed conductance decrease of their RGO sensor upon DNA hybridization.[228] In that work, a secondary RGO sensor was used as the internal reference to cancel out the common interference, such as pH change and nonspecific biological adhesion. Choi *et al*. presented a DNA sensor using sulfonated reduced graphene oxide (srGO) through microwave-assisted sulfonation.[99] The $-SO_3$ group on srGO surface provides strong binding sites for immobilization of probe ssDNA. In addition, the srGO sheets can be readily dispersed in water without using a dispersion agent and therefore can be readily deposited on a substrate as a uniform ultrathin layer for device fabrication. Consistently, DNA hybridization also caused decrease of srGO conductance.

5.5 Cellular detection

In recent years, nanoelectronic biosensors based on 1D semiconducting nanostructures (carbon nanotubes and silicon nanowires) have been coupled with live cells to detect their low presence and dynamic activities.[140,179–181,229–231] Owing to its unique properties, graphene adds a new dimension to the nanoelectronics–cell interface. As a cell membrane is also a 2D structure (5 nm-thick lipid bilayer), it can intimately interact with flat graphene. In contrast, when a cell membrane interfaces with other nanostructures, the interaction may not be tight and homogeneous and the local curvature induced on the thin cell membrane by nanotopographic structures may alter cell functions in intriguing ways.[232] Given the close interaction between the cell membrane and graphene as well as the highly sensitive nature of graphene's electrical properties, the cell-activity-induced local electrical and chemical fluctuations in the nanogap between graphene and cell membrane could significantly change the graphene conductance.

Silicon nanowires[179,233,234] and carbon nanotube transistors[229] have been used to detect cellular bioelectricity (action potentials) resulting from the orchestrated activities of membrane ion channels. Lieber and co-workers recently demonstrated a graphene FET to extracellularly detect action potentials from single electrogenic cardiomyocytes (Fig. 7a).[235] Mechanically

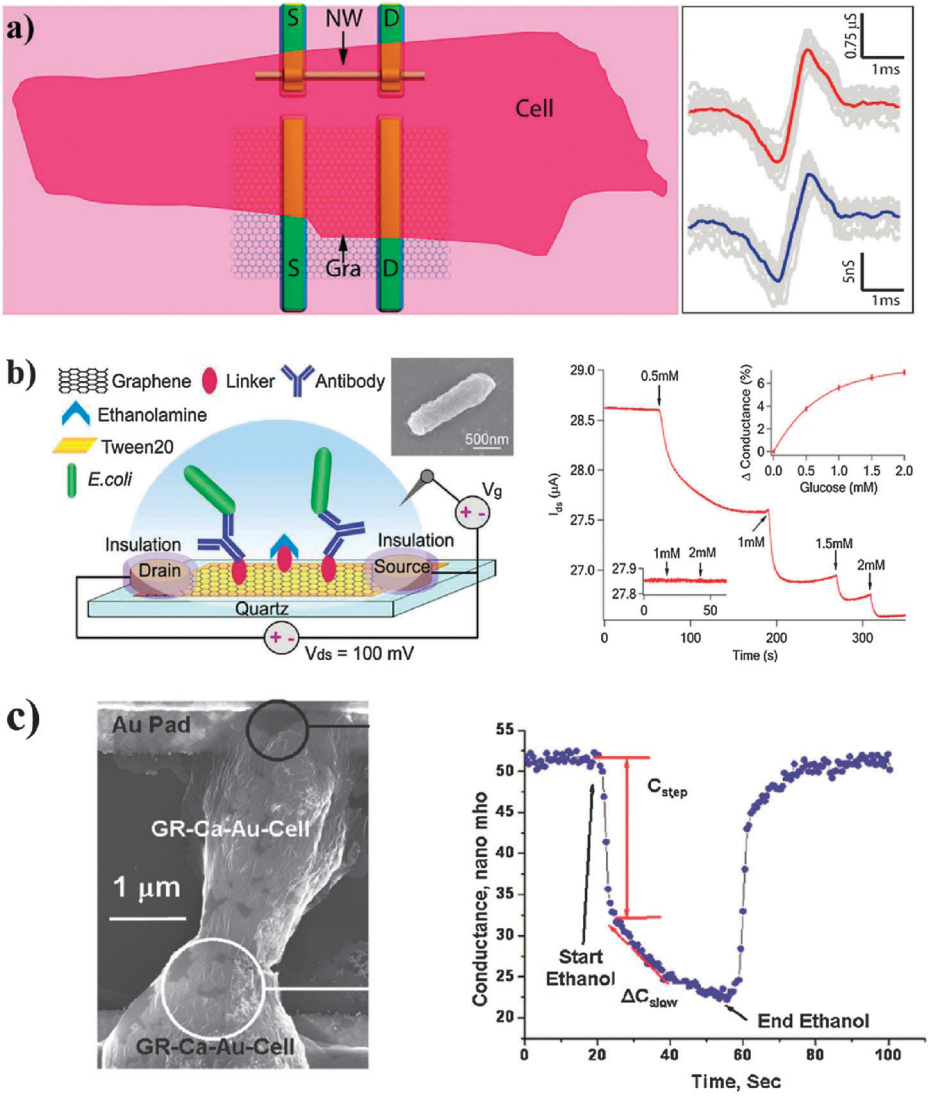

Fig. 7 Electronic graphene sensors for cellular detection. (a) Detection of cellular bioelectricity. Left: representation of a cardiomyocyte cell interfaced to a graphene-FET and a silicon nanowire-FET device; right: thirteen electrical signals (gray traces) from the graphene-FET (upper data) and the silicon nanowire-FET (lower data) devices in response to the spontaneous action potentials produced by the cardiomyocyte. The peaks were aligned in time and the average was plotted in red and blue, respectively. Adapted from ref. 235. Copyright 2010 American Chemical Society. (b) Detecting bacteria and their metabolic activity. Left: illustration of an anti-*E. coli* antibody functionalized graphene-FET for detection of *E. coli*. Inset: scanning electron microscopy (SEM) image of an *E. coli* on antibody functionalized CVD-graphene. Right: real-time current recording (V_{ds} = 100 mV and V_g = 0 V) of a bacteria-bound graphene device with application of glucose at different concentrations. Lower inset: bacteria free graphene sensor was not responsive to glucose. Upper inset: Percentage change in graphene conductance *versus* glucose concentration. Adapted from ref. 105. Copyright 2011 the Royal Society of Chemistry. (c) Electromechanical interface between graphene and yeast cell. Left: SEM image showing two RGO covered yeast cells spanning the gap between Au electrodes. GR = RGO. Right: real-time recording of the conductance change of the RGO layer on cell (biased at 100 mV) when the yeast cell was exposed to ethanol (99%) for 40 s. A reversible drop in conductance was observed. Adapted from ref. 240. Copyright 2011 American Chemical Society.

exfoliated graphene was used to fabricate devices by e-beam lithography. The authors showed that the sensitivity of graphene FET is superior to conventional metallic microelectrodes and comparable to a silicon nanowire FET. The device response is triggered by the field-effect due to the change of electrical potential at the nano-interface between the cell and the FET while the ionic current through the membrane ion channels flows in the resistive solution in the nano-interface. Although the field-effect of graphene is less prominent than silicon nanowires, a comparable signal-to-noise ratio was obtained by a graphene FET. This may be attributable to its much larger interfacing area with the cell. It would be interesting to see the performance of graphene nanoribbons (GNRs) with large bandgap in detection of cellular bioelectricity. Supposedly, GNRs are able to provide both high sensitivity because of their prominent field-effect and high spatial resolution because of their nanoscale lateral dimension.

In a work by He *et al.*, centimetre-long, micrometre-wide, ultrathin and continuous RGO network films were made using microfluidic patterning and coupled with neuroendocrine

PC12 cells.[236] Such readily fabricated RGO FETs were able to detect rapid vesicular secretion of hormone catecholamines from PC12 cells triggered by membrane depolarization. Catecholamine molecules released into the membrane–FET nanogap interact with RGO sheets through π–π interaction, and increase p-type RGO conductance *via* p-doping. The specificity of detection is achieved in the well-defined biological context, in this case, the highly regulated stimulus-secretion coupling. As compared to electrophysiological single cell recordings,[237,238] this nanoelectronic approach is non-invasive and does not require high experimental skills. As also demonstrated by the authors, microfluidic patterned RGO thin-film devices can be made on flexible substrates that could conform onto a curved target (*e.g.*, an organ).

Coupling between graphene FETs and bacteria has also been demonstrated for detection of the presence and activities of bacteria. The bacteria sensor demonstrated by Mohanty and Berry used a microsized amine-modified graphene (GA) sheet as the sensing material.[100] The GA was synthesized by either exfoliation of ammonia plasma-treated graphite flakes or exposing GO sheets to hydrogen plasma followed by ammonia or nitrogen plasma. Significant conductance increase was observed upon attachment of single bacterium which imposes prominent p-doping to the GA sheet (*ca.* ~1400 conducting holes per bacterium). The high sensitivity may be ascribed to the high hole mobility of GA and the firm interaction between the positively charged amino groups on GA and the highly negatively charged bacterial wall. However, this sensor is not practical because the detection relied on non-specific electrostatic adhesion of bacteria without discrimination of bacterial species and the measurement was non-physiologically conducted in a dry nitrogen atmosphere.

Chen and co-workers recently demonstrated a CVD-grown graphene based sensor to specifically and sensitively detect *E. coli* bacteria in solution (Fig. 7b).[105] Graphene was functionalized with anti-*E. coli* antibodies as the recognition element, and non-specific attachment of other bacteria species or molecules was prevented by coating of a passivation layer. *E. coli* at a concentration as low as 10 cfu ml^{-1} can be detected while a different bacteria species at a much higher concentration cannot produce a significant signal. The detection is based on the field-effect caused by the highly negatively charged bacterial wall. The detection limit of this graphene sensor is much better than the sensor made with a similarly sized thin-film network of single-walled carbon nanotubes.[239] Furthermore, the authors showed that the graphene FETs are able to detect the glucose induced metabolic activities of the bound *E. coli* bacteria in real time. It was hypothesized that discharge of organic acids (metabolites) into the nano-gap between the graphene and the interfacing bacterial surface decreases the local pH and consequently the graphene conductance.

Electromechanical coupling between graphene and yeast cell was recently reported.[240] In this interesting work, RGO microsheets were coated on the cell surface forming an electrically conductive layer (Fig. 7c). By monitoring the electrical conductance of the RGO layer, the dynamic mechanical response of a yeast cell to osmotic stresses or heat shock can be recorded in real-time, because a change in the cell volume leads to straining of the RGO sheets and consequent formation of wrinkles that reduces the electrical conductivity of RGO layer. The ultrathin thickness makes the RGO sheet highly sensitive to structural deformation.[196]

Evidently from the examples discussed in this section, graphene electronic sensors promise applications in rapid detection of rare pathogenic microbes or pathological cells (*e.g.*, cancer cells), high throughput studies of dynamic cell functions, and high throughput drug screening targeting on those cell functions.

5.6 Integrating biomimetic membranes with graphene FETs for biosensing

Cell membranes are perplexingly complex, crowded with a huge variety of molecular machines (membrane proteins). To enable the study of membrane protein activities in the simplest native environment, integration of an artificial lipid bilayer (biomimetic membrane) with carbon nanotube FETs has been demonstrated.[241,242] Presumably, the flat and size-tunable graphene is a better alternative to interface with (support) biomimetic membranes for biosensing, in particular, examining the functions of molecules that operate in or on cell membranes, or disrupt cell membranes.

Ang *et al.* deposited a gram-negative bacteria biomimetic membrane on a CVD grown graphene film.[243] And this hybrid device was used to detect magainin 2, which is an antimicrobial agent secreted by skin cells of African frog (Fig. 8). Magainin 2 disrupts the thin biomimetic membrane by dislodging the upper layer of the lipid from the surface. The thinning of membrane thickness from *ca.* 5 nm to *ca.* 3 nm reduced the field-effect from the negatively charged lower membrane layer because of the charge screening by the ionic solution within the Debye distance. A low detection limit was achieved at 100 pM with a large Dirac point shift (50 mV). Such a graphene sensor opens a new route to study disruptions or functions of cell membranes (*e.g.*, drug cytotoxicity, ligand–receptor interaction, or ion channel activities).

5.7 Improving the performance of graphene electronic sensors

Graphene based nanoelectronic sensors are only emerging. Strategies can be devised to further improve their performance. For example, Cheng *et al.* showed that suspending the graphene sheet by etching away the underneath silicon oxide reduces the low-frequency noise originated from the graphene–substrate contact, leading to an improvement of the signal-to-noise by 14 dB for both holes and electrons.[244] In addition, since the scattering effect from the substrate is removed, the device sensitivity (transconductance) increases by 1.5–2 times. Dankerl *et al.* have fabricated a graphene FET array on epitaxially grown graphene on SiC.[245] Individually addressable graphene FETs in the array could be differentially functionalized for simultaneous detection of multiple targets for high throughput and information-rich analyses. The throughput and performance of graphene electronic sensors may be further improved by the integration with micro/nanofluidics.[246]

Electronic sensors based on a single graphene nanoribbon (GNR) or quantum dot are anticipated to offer high sensitivity and high spatial resolution. As an example, Min *et al.* theoretically demonstrated a GNR based DNA sequencing device, in which a GNR is suspended on top of a fluidic nanochannel.[247] When a ssDNA is electrophoretically threaded through the

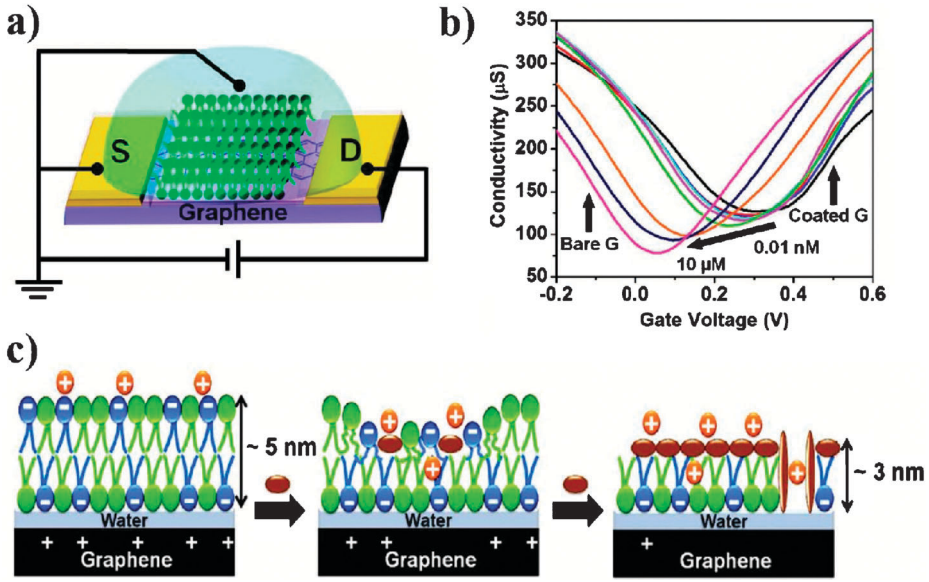

Fig. 8 Integrating a biomimetic membrane with a graphene FET for biosensing. (a) Schematic representation of biomimetic membrane-CVD grown graphene field-effect transistor. (b) Transfer curves of a biomimetic membrane-CVD grown graphene FET with increasing magainin 2 concentrations. (c) Schematic diagram showing the sensing concept of membrane thinning effect by magainin 2 (brown ovals). Adapted with permission from ref. 243. Copyright 2010 American Chemical Society.

nanochannel, electrical signatures of four types of nucleotides can be resolved because (1) the narrow width of GNR is comparable to the size of a base and (2) the ballistic conductance of GNR diminishes at specific energies corresponding to the characteristic π-molecular orbitals *via* Fano resonance. The authors also argued that narrow GNRs are superior to carbon nanotubes whose multiple conductance levels and multiple stacking reduce the characteristic electrical perturbations by the bases over the noise level. Recently, Dong *et al.*[248] showed that the network of RGO nanoribbons obtained by chemically unzipping multiwalled carbon nanotubes exhibits a higher on/off ratio than graphene or rGO film and a significantly higher sensitivity in electrically detecting adenosine triphosphate (ATP) molecules as compared to that of the single-walled carbon nanotube (SWCNT) network.[249]

Use of smaller recognition elements (*e.g.*, antigen-binding fragment of antibodies) to bring the targets closer to graphene should also enhance the sensitivity. As a novel alternative, artificial receptors could be created on graphene using molecular imprinting (MIP),[250] which involves polymerization around the template (target) molecules and subsequent wash-away of the templates (leaving the artificial or synthetic binding sites open for the specific binding with the target molecules). MIP has been employed for carbon nanotube based biosensors.[251] We speculate that a flat graphene sheet is more suitable for uniform and effective MIP in comparison with small nanotubes. Such artificial receptors ensure direct contact between the graphene and the targets, high specificity, and robustness.

6. Optical sensors

Graphene oxides exhibit interesting optical properties.[61] Unlike zero-gap graphene or other carbonaceous materials, GO can fluoresce in a wide range of wavelength (from near-infrared to ultraviolet).[252] This is because the disordered oxygenated functional groups on GO confine π electrons within the sp^2-carbon nanodomains, thereby giving rise to a local energy gap that inversely scales with the domain size. Therefore, GO has the potential to serve as a universal fluorescence label for optical imaging.[253] Interestingly, just like other graphitic materials, GO is also capable of quenching fluorescence.[254] The quenching efficiency of GO is superior to the conventional organic quenchers. It has been shown that quenching even at a distance of 30 nm is attainable by GO.[255] On the basis of its fluorescence and quenching abilities, GO can serve as either an energy donor or acceptor in a fluorescence resonance energy transfer (FRET) sensor. The optical characteristics (*e.g.*, fluorescence wavelength and quenching efficiency) of GO is tunable by controlling the extent and type of its oxygenation.[255–257]

Graphene materials may also assist to enhance the performance of optical sensors, by increasing the signal-to-noise ratio, loading of the recognition element, adsorption of the target molecules, efficiency of signal transduction, *etc.* For example, taking advantage of their quenching properties, graphene materials can be used to reduce fluorescence interference in Raman spectroscopy[258] and enhance the Raman signal through charge transfer with the adsorbed molecules.[259] Other merits of graphene materials (GO in particular) may also be useful for optical sensors, such as high optical transparency, high surface-to-volume ratio, the ability to intimately interact with many molecules *via* π–π or electrostatic or hydrophobic interaction, the ability to catalyze luminescence-generating or signal-transduction reaction, and so on.

6.1 As the sensing element in FRET

GO based FRET sensors may consist of three components: a recognition probe (*e.g.*, probe ssDNA that hybridizes with target ssDNA, or aptamer, an oligonucleic acid that binds with a specific target molecule), a reporter fluorophore conjugated on the probe, and GO. Initially, the fluorescently tagged probes

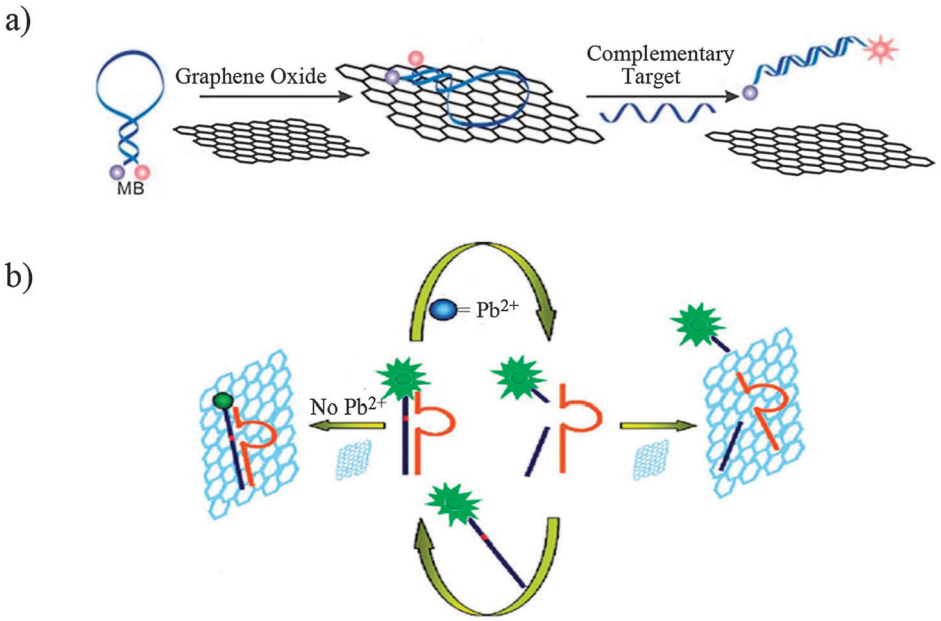

Fig. 9 GO as the quencher in a FRET sensor. (a) Schematic illustration of DNA hybridization using a double-quenching system consisting of GO and molecular beacon (MB). Adapted with permission from ref. 263. Copyright 2010 the Royal Society of Chemistry. (b) Schematic illustration of the DNAzyme-GO based fluorescence sensor for detection of Pb^{2+}. Adapted with permission from ref. 281. Copyright 2011 American Chemical Society.

attach firmly onto GO through strong π–π interaction between nucleobases and GO plane. The close interaction leads to fluorescence quenching. Binding of the detection targets then causes a conformational change of the probe, which, in turn, leads to dissociation of the probe from the GO surface. And the subsequent termination of FRET restores the fluorescence of the initially quenched fluorophores. This kind of mix-and-detect sensors is convenient and cheap. Tang *et al.* reported such a GO based fluorescence quenching-recovery sensor to detect ssDNA with a LOD of nM range.[260] The authors also showed that their sensors can perform even in the presence of DNAase because ssDNA retained on the GO surface was found to be indigestible by DNAase. Two similar DNA sensors, which are also able to distinguish single-base-mismatch, have also been demonstrated.[261,262]

In order to further improve the sensitivity, Li *et al.* designed a double-quenching system combining GO and molecular beacon (MB—a hairpin-structured oligonucleotide conjugated with a FRET pair) (Fig. 9a).[263] Relief of both GO quenching and intra-probe quenching of MB upon binding of the complementary DNAs greatly enhances the signal-to-noise ratio, resulting in a low LOD of 0.1 nM. Due to the high thermal stability of MB–GO complex, this sensor can operate at a high temperature (75 °C), promising its use in polymer chain reaction (PCR). Alternatively, Dong *et al.* employed CdTe quantum dot (QD) as the fluorescence reporter to construct GO/MB-QD sensing platform.[264] The mercaptoacetic acid (MPA)-capped CdTe QD served as a core for adsorption of multiple MBs to form a probe complex. It is worth mentioning that, compared with commonly used organic fluorophores, QD possesses many advantages including high quantum yield, high photostability, and size-tunable absorption and emission.[265]

Using similar detection scheme and particularly designed aptamer receptors, proteins and metal ions have also been detected. Based on the GO–aptamer system, Lu *et al.* devised a human thrombin sensor with a nM detection limit,[266] which excels regular dye–quencher pair labeled aptamers[267] and is comparable to aptamer–CNT based optical sensors.[268] Another thrombin sensor with a lower detection limit (pM level) was demonstrated, using surfactant dispersed RGO instead of GO.[269] A GO-FRET sensor to detect Cyclin A2—an early-stage cancer indicator—has been shown.[270] The achieved LOD of 0.5 nM is 10-fold lower than that of SWCNT based sensors. Notably, for the first time, Wang *et al.* reported an intracellular molecular sensor using the GO-FRET scheme for detection of intracellular ATP molecules.[271] They showed that GO nanosheets (~100 nm) attached with fluorescent ATP-specific aptamers can be readily uptaken by the mice epithelial cells without introducing apparent cytotoxicity, because of the small size, high solubility, and biocompatability of GO nanosheets. In addition, in agreement with a previous observation,[260] the GO sheets also protect the aptamer probes from being cleaved by the intracellular enzymes.

Wen *et al.* developed an Ag^+ sensor with a LOD of 5 nM by employing a fluorescence labelled Ag^+-specific aptamer (cytosine-rich oligonucleotide) as the probe.[272] Association of Ag^+ ions with the cytosine bases induces the conformational change of the probe and yields a rigid hairpin structure. This leads to an increase of the distance between the GO sheet and the fluorophore beyond the effective quenching region, hence, termination of FRET. In the practical tests of river water, the sensor exhibits excellent specificity against various interferences (*e.g.* other ion species and particles) and its LOD satisfies the requirement of US Environmental Protection Agency (EPA) for drinking water.

FRET sensors with different detection schemes have been explored. For example, He *et al.* demonstrated a DNA sensor by using 'post-mixing method', in which fluorescent probe-ssDNAs

were first mixed with target-ssDNAs followed by addition of GO sheets.[273] Because the fluorescence of the unhybridized probes is effectively quenched by GO sheets, the remained fluorescence intensity from the hybridized probes indicates the concentration of target DNAs. Using this post-mixing method, the reaction time is largely reduced due to the absence of competition between the interaction of GO/probe DNA and the interaction of probe DNA/target DNA. Furthermore, in this study, different probe DNAs with distinctly coloured fluorophores were co-decorated on GO sheets in order to simultaneously detect multiple DNA targets. The interference between different probe DNAs was found to be negligible. The detection limit of such multicoloured DNA sensors can reach as low as 100 pM. It outperforms the previously reported FRET sensors based on molecular beacons[274,275] or other nanomaterials.[276,277]

Instead of using ssDNA or aptamer as the recognition element, Balapanuru *et al.* used organic dye 4-(1-pyrenylvinyl)-*N*-butylpyridinium cation (PNP^+) as the probe for dsDNA.[278] Electrostatic interaction between negatively charged dsDNAs and positively charged PNP^+ is able to remove PNP^+ from the GO surface and cause quench recovery. Cai *et al.* used a butterfly-shaped conjugated oligoelectrolyte as the FRET donor and receptor to specifically detect heparin (a glycosaminoglycan).[279] Using upconverting phosphors (UCP) as the donor and conjugated concanavalin A as the receptor, a GO-FRET sensor was developed for detection of glucose in human serum samples.[280] In a novel work by Zhao *et al.*, a GO-FRET sensor for detection of Pb^{2+} ions was developed using the hybrid of DNAzyme and fluorescence labelled substrate DNA as the recognition element (Fig. 9b).[281] The DNAzyme–substrate DNA complex was brought onto the GO surface *via* π–π interaction between GO and the large loop sequence on DNAzyme. Once Pb^{2+} is introduced, it activates the DNAzyme to cleave the substrate strand into two parts, releasing a short fluorophore-linked oligonucleotide fragment which is too short to attach back onto GO again. Consequently, the fluorescence is recovered from quenching. The reaction also releases DNAzyme from the GO surface, allowing it to hybridize with another bound substrate DNA and thus providing an amplified signal for Pb^{2+} detection. This sensor is able to detect Pb^{2+} at a concentration as low as 300 pM with a selectivity 2 orders higher than other heavy metal ions. The similar strategy was used by Wen *et al.*[282] Based on the finding that Pb^{2+} could specifically modulate the interaction between GO and a Pb^{2+} dependent 8–17 DNAzyme *via* cleavage of the 17S substrate, a simple mix-and-detect Pb^{2+} sensor was developed. In the presence of Pb^{2+}, the substrate DNA strand is specifically and irreversibly cleaved at the cleavage site of 17S substrate, resulting in the disassembly of the duplex DNAzyme into three ssDNA fragments: the 3′- and 5′-fragments of the substrate strand and the enzyme strand. These ssDNAs could be adsorbed onto GO nanosheets *via* π–π stacking between the bases and the aromatic structure of GO and consequently the dye modified DNAs were quenched. This Pb^{2+} sensor gives a LOD of 0.5 nM.

Instead of using GO as the FRET quencher, Liu and colleagues used GO as the energy donor in their FRET sensor for detection of ssDNA.[283] Gold nanoparticles (AuNPs), which served as the energy acceptor (fluorescence quencher), were conjugated on the target ssDNA. When the target ssDNA hybridizes with the probe DNA covalently linked on the GO surface, AuNPs brought onto the GO surface quench the fluorescence of GO. Using a similar AuNP quenching scheme, a sensor for detection of rotavirus was also demonstrated (Fig. 10).[284] Firstly, rotavirus-specific antibodies were covalently immobilized on the GO surface. After rotaviruses were fetched by the antibodies, the complex of the secondary rotavirus-antibody/DNA/AuNP was added to form a sandwich structure, causing quenching of GO fluorescence by AuNPs. This immune-pathogen sensor with high selectivity, sensitivity ($\sim$1000 pfu ml^{-1}) and rapid detection time could be a promising alternative to the conventional time-consuming pathogen detection methods.

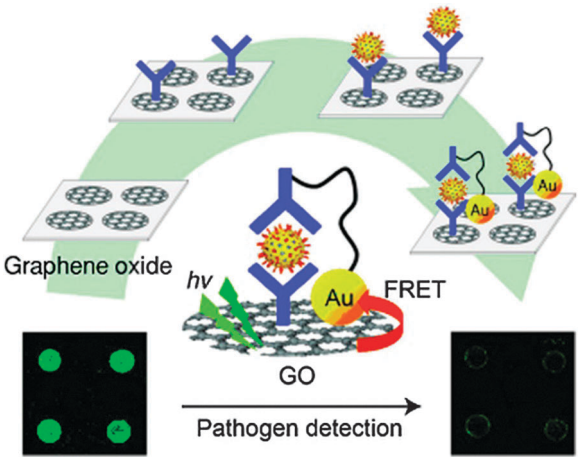

Fig. 10 GO as the fluorescence donor in a FRET sensor for immunodetection of pathogens. Adapted with permission from ref. 284. Copyright 2010 Wiley-VCH Verlag GmbH & Co. KGaA, Weinheim.

6.2 As a facilitator in optical sensors

Instead of serving as the (or a part of) sensing element, graphene materials may also be used to improve the performance of optical sensors. Wu *et al.* theoretically proposed that graphene can improve the performance of surface plasmon resonance (SPR) based biosensors.[285] Firstly, the coated graphene can enhance adsorption of biomolecules onto the metal/dielectric interface at which the surface electromagnetic wave propagates. Secondly, multi-graphene layers can increase the sensitivity of SPR response. Choi *et al.* also theoretically demonstrate that the graphene-on-silver substrate can enhance the SPR sensitivity by 3 times in comparison with the conventional gold-film-based SPR biosensor.[286] In addition, graphene can prevent oxidation of silver due to its high impermeability to oxygen. Wang *et al.* fabricated a label-free, regenerative and sensitive SPR sensor to detect α-thrombin with an ultralow detection limit of 50 pM.[287] The thrombin aptamer (TBA) is noncovalently adsorbed on the RGO layer, which is assembled on a positively charged SPR Au (p-Au) film *via* electrostatic interaction. When TBA fetches the target molecule (α-thrombin), it detaches from the RGO, producing an obvious SPR angle decrease. The authors also illustrated that such SPR sensors exhibit excellent selectivity and can be applied in real biological fluid (1% pretreated human plasma).

Cd^{2+} can be detected based on absorbance change upon its binding with 5,10,15,20-tetrakis (1-methyl-4-pyridinio)

porphyrin (TMPyP). It has been demonstrated that RGO can accelerate this binding reaction by 150 times because RGO sheets are able to flatten TMPyP through electrostatic and the π–π interaction with porphyrin rings on TMPyP and facilitate the coordination reaction between Cd^{2+} ions and TMPyP.[288] Glucose can be detected based on absorbance change of 3,3,5,5-tetramethylbenzidine (TMB) when it is oxidized by H_2O_2—the product of glucose oxidation by glucose oxidase. Song *et al*. showed that COOH–GO, which was synthesized by adding NaOH and chloroaceticacid into GO suspension, exhibits intrinsic peroxidase catalytic activity (higher than that of horseradish peroxidase); and COOH–GO can serve as an intermediate to transfer electrons from TMB to H_2O_2.[289] High catalytic activity, high affinity to organic substrates, ease of preparation, low-cost and excellent stability makes COOH–GO a better choice to facilitate TMB based glucose detection, compared with other peroxidases (*e.g*., horseradish peroxidase or Fe_3O_4 nanoparticles).

In an electrochemiluminescence sensor for detection of glutathione (a cellular antioxidant), GO sheets were added in the solution to amplify electrogenerated chemiluminescence (ECL) by facilitating the generation of quantum dot radicals and oxygen radicals.[290] The authors argued that GO with a wide range of energy bandgaps serves as a good intermedium for electron transfer. The sensor, with a LOD of 8.3 μM, was successfully employed to assess real samples (glutathione-containing eye drug). In an ECL sensor for detection of prostate protein antigen (prostate cancer marker), RGO sheets were used as the electrode material to enhance the ECL reaction taking advantage of its excellent electrocatalytic and conductive properties.[291]

In the work by Lu *et al*., a silver nanoparticle (AgNP) decorated RGO film was used as the substrate for surface enhanced Raman scattering (SERS) to detect aromatic molecules.[292] A LOD of nM range was obtained because of the ability of RGO to enhance the Raman signal and quench the fluorescence background and the high adsorption efficiency of RGO towards aromatic compounds. Ren *et al*. reported a SERS sensor for detection of folic acid molecules.[293] PDDA-functionalized GO and AgNPs were used as the substrate and a low LOD of 9 nM was attained in both water and diluted human serum.

7. Nanopore sensors

A nanopore, which resides on an insulating membrane and has a molecular diameter, can be used as a molecular detector with exquisite (single molecule or even intra-molecular) sensitivity. When a molecule passes through a narrow pore that connects two separated electrolyte solutions, the ionic current flowing through the pore is partially blocked, producing a current signature influenced by the charge state and subtle molecular structure of the occupying molecule or its segment. Protein nanopores embedded within a lipid bilayer have been used first for detection of DNA and RNA molecules.[294] And the discovery that the base composition of a DNA/RNA molecule affects the signal of current blockage[295] has invited tremendous interests in developing nanopore-based ultra-fast DNA sequencing techniques. To overcome the poor stability and durability of biological nanopores, solid-state nanopores created on dielectric membranes (*e.g*., Si_3N_4 or SiO_2) have been developed.[296,297] However, an essential requirement for nanopores to achieve single-base sensitivity for DNA sequencing is that the nanopore membrane has to be thinner than or as thin as the distance between the two successive bases (0.34 nm which is about an atom apart). This is much smaller than the thickness of lipid bilayer (~5 nm) and the currently achievable thickness of dielectric membranes. Graphene, the thinnest material known in the world, makes nanopore-sequencing an attainable possibility. In addition, the extraordinary mechanical stiffness and chemical stability of graphene assure the manufacturability and durability of a free-standing graphene film with created nanopore(s).

Using electron beam drilling, Merchant *et al*. fabricated a nanopore (5–10 nm in diameter) on CVD-grown few-layered graphene sheets (3–5 layers), which was suspended on a micrometre-hole on silicon nitride membrane (Fig. 11).[298] In addition, a titanium dioxide nanolayer was coated on the graphene surface to make a cleaner and more wettable pore, and consequently, to reduce the current noise.[296] However, this comes with a price of increased pore thickness. To reduce the thickness of graphene nanopore, Schneider *et al*. used a single-layered and un-coated graphene sheet obtained from mechanical exfoliation[299] and Garaj *et al*. used one- or double-layered CVD grown graphene.[300] The graphene nanopores produce a larger current blockage upon DNA translocation than that from the conventional solid-state nanopores because of the ultrathin nature of the graphene nanopores. And despite its atomic thickness, graphene is a remarkable ionic insulator.

Although graphene nanopores promise for spatially-resolved detection of individual nucleotides, they just like other nanopores still face several challenges in order to practically realize DNA sequencing. These include fast translocation velocity of DNA driven by the intense electrical field, low bandwidth in recording of ionic-current, low signal magnitude due to slow mobility of ions and blockage based detection scheme.[301] Nelson *et al*. proposed a graphene nanopore drilled on a graphene nanoribbon (GNR) FET (Fig. 12a).[302] They demonstrated theoretically that when ssDNA is traveling through the nanopore, the GNR conductance changes due to modulation in current tunneling across the pore and the field-effect due to electrostatic interaction of the nucleotide with the ribbon. Different types of nucleotides can be distinguished due to their characteristic energy levels and characteristic interactions with the nanoribbon, suggesting the feasibility of rapid DNA sequencing. The signal response from such electronic-conductance-based nanopore sensors is several orders higher than the ionic-current-based nanopore sensors (mA *vs*. nA). The high sensitivity is attributable to the new sensing mechanism, high carrier mobility of graphene, and large energy bandgap provided by GNR. In another study, it was argued that the sensitivity could be further improved if the nanopore is created at the edge of the GNR in order to take advantage of its edge-sensitivity.[303]

It has been theoretically proven that a graphene nanogap (gap width ~1.0–1.5 nm) can be used to electrically read the base sequence of a single DNA molecule based on change of tunneling current across the gap, which is sensitive to the characteristic local electronic densities of different nucleotides.[304]

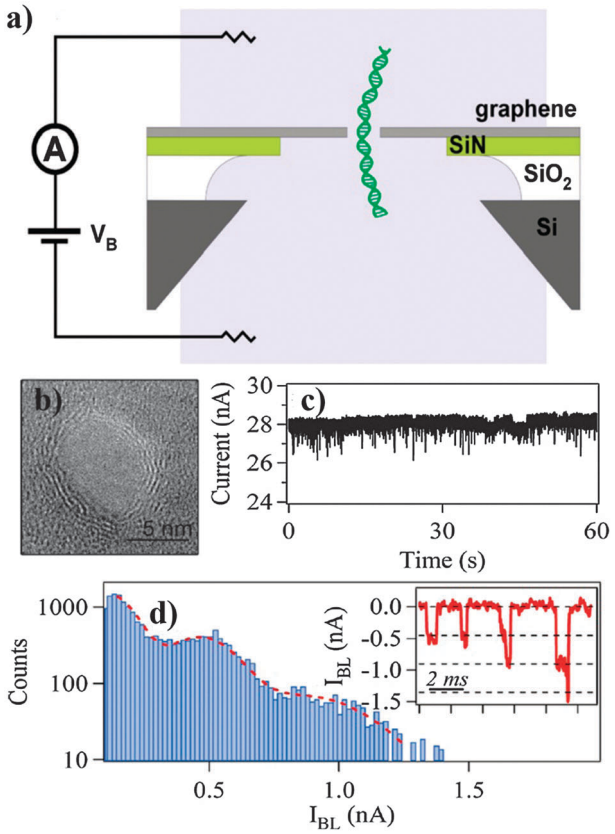

Fig. 11 Graphene nanopore for detection of a single DNA molecule. (a) Illustration of few-layer graphene (1–5 nm thick) suspended over a 1 μm diameter hole in a 40 nm thick silicon nitride (SiN) membrane. The SiN membrane is suspended over an approximately 50 × 50 μm^2 aperture in a silicon chip coated with a 5 μm SiO_2 layer. The device is inserted into a PDMS measurement cell with microfluidic channels that form reservoirs in contact with either side of the chip. A bias voltage, V_B, is applied between the reservoirs to drive DNA through the nanopore. (b) TEM image of an ~8 nm graphene nanopore. (c) DNA translocation events as signaled by discrete ionic current blockages. (d) Histogram of blocked currents for measured translocation events for the device at V_B = 100 mV in 1 M KCl solution. Data are fit using two Gaussian functions with mean values at 0.45 and 0.90 nA. Inset displays concatenated events caused by unfolded or folded translocating DNA molecules. Blocked current signal (I_{BL}) values of 0.45, 0.9, and 1.35 nA are indicated with dashed black lines, indicating unfolded, singly folded, and doubly folded entries, respectively. Adapted with permission from ref. 298. Copyright 2010 American Chemical Society.

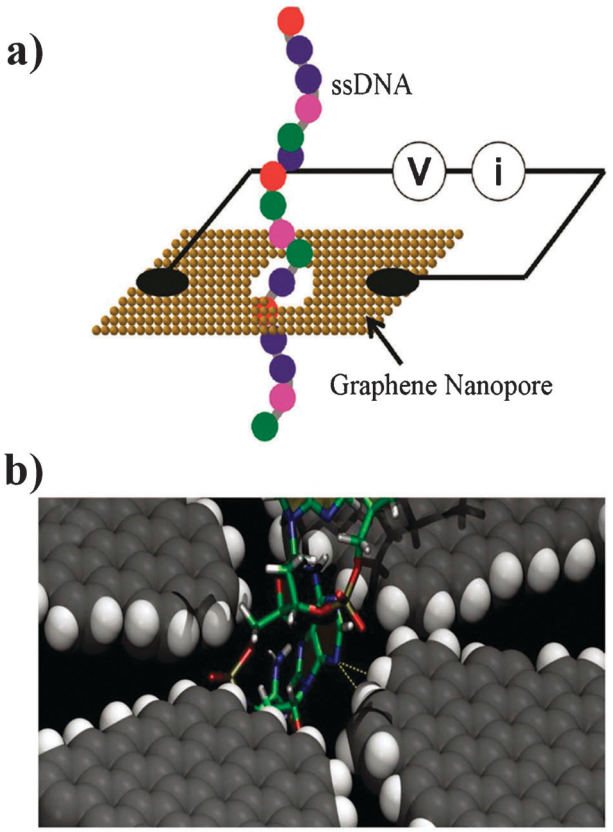

Fig. 12 Graphene nanopore for rapid DNA sequencing. (a) Illustration of translocation of a ssDNA through a graphene nanopore while the electronic current in graphene is monitored. Adapted with permission from ref. 302. Copyright 2010 American Chemical Society. (b) Snapshot extracted from the molecular dynamics simulation of ssDNA translocation through a graphene nanopore, showing a moment when two H-bonds (dotted yellow lines) are formed simultaneously between the nitrogen atom of a DNA nucleobase and two H atoms attached to the graphene-edge. Adapted with permission from ref. 305. Copyright 2011 Wiley-VCH Verlag GmbH & Co. KGaA, Weinheim.

Inspired by this idea, He *et al*. proposed a graphene nanopore defined by four graphene nanoelectrodes, which may be fabricated by e-beam etching on a graphene film deposited on a thin substrate (Fig. 12b).[305] Transverse tunneling conductance is recorded between two opposite nanoelectrodes when an ssDNA is electrophoretically driven through the nanopore. The hydrogenated edges of the four electrodes couple with the DNA base *via* a hydrogen bond, which slows down the DNA translocation velocity and enhances the electron tunneling rate over vacuum tunneling. The hydrogen bonding thus can increase the average transverse conductivity by about 3 orders of magnitude with reduced statistical variance. With novel design of pore formation[306] and functionalization,[307] graphene nanopore techniques would advance further for DNA sequencing or single molecule characterization in general.

8. Conclusions and outlook

In spite of its very short history, graphene has already demonstrated great successes in biological and chemical sensing. Because of the availability of a spectrum of graphene materials and their pluripotent sensing capabilities, graphene based sensors have already been employed for a dazzling diversity of targets ranging from gaseous molecules, small chemicals and ions, biological molecules (*e.g*., sugars, proteins, DNAs), bacterial and animal cells, as well as dynamic cellular activities. These sensors exhibit outstanding performance as compared with the state-of-the-art techniques, in terms of sensitivity, selectivity, detection range, temporal resolution, reproducibility, response time, or cost. Although most of these developments are merely proof-of-concept demonstrations, as a step forward to the practical or commercialized uses, some of them

have been proven to be functional for complex real samples, for example, serum samples.

Without a doubt, the full potential of graphene based sensors is far from being reached. Some graphene materials (*e.g.*, GNR, graphene QD, bilayered graphene) have barely been explored for sensor applications so far, although their potentials are highly anticipated due to their exceptional properties. And new graphene materials and structures are still emerging, for instances, graphane (a hydrogenated twin material of graphene)[308] and CVD-grown three-dimensional graphene foam.[309] Hybridizing or compositing graphene materials with various organic and inorganic systems (such as polymers, carbon nanotubes, nanoparticles)[108,309–312] are also extending the arsenal for graphene sensor development. By combing its different capabilities and merits, a graphene sensor that is equipped with multiple sensing modalities (*e.g.*, electronic and optical) shall be possible. And a graphene sensor that is able to detect a single biomolecule shall not be far-reaching. Taken together, the abilities and applications of graphene sensors are only limited by imagination.

Currently, the development and widespread application of graphene sensors are largely hindered by the lack of methods for controllable, reproducible, scalable, and facile preparation of graphene materials with defined structures and properties.[67] In addition, a better understanding of graphene properties, the interactions between graphene and molecules/cells, and the detection (or signal transduction) mechanisms is critical. To move forward, the collaborations between different disciplines and technologies are necessary. In witness of their current explosive development, we envision that the emerging graphene sensors would soon bring significant impacts on environmental and safety monitoring, diagnosis, biological studies, and drug screening.

References

1 D. S. L. Abergel, V. Apalkov, J. Berashevich, K. Ziegler and T. Chakraborty, *Adv. Phys.*, 2010, **59**, 261–482.
2 M. J. Allen, V. C. Tung and R. B. Kaner, *Chem. Rev.*, 2010, **110**, 132–145.
3 M. F. Craciun, S. Russo, M. Yamamoto and S. Tarucha, *Nano Today*, 2011, **6**, 42–60.
4 C. N. R. Rao, K. Biswas, K. S. Subrahmanyam and A. Govindaraj, *J. Mater. Chem.*, 2009, **19**, 2457–2469.
5 V. Singh, D. Joung, L. Zhai, S. Das, S. I. Khondaker and S. Seal, *Prog. Mater. Sci.*, 2011, **56**, 1178–1271.
6 Y. Q. Wu, Y. M. Lin, A. A. Bol, K. A. Jenkins, F. N. Xia, D. B. Farmer, Y. Zhu and P. Avouris, *Nature*, 2011, **472**, 74–78.
7 F. S. F. Schwierz, *Nat. Nanotechnol.*, 2010, **5**, 487–496.
8 J. S. Wu, W. Pisula and K. Mullen, *Chem. Rev.*, 2007, **107**, 718–747.
9 Y. Q. Sun, Q. O. Wu and G. Q. Shi, *Energy Environ. Sci.*, 2011, **4**, 1113–1132.
10 D. A. C. Brownson, D. K. Kampouris and C. E. Banks, *J. Power Sources*, 2011, **196**, 4873–4885.
11 C. K. Huang, Y. X. Ou, Y. Q. Bie, Q. Zhao and D. P. Yu, *Appl. Phys. Lett.*, 2011, **98**, 263104.
12 Z. S. Wu, S. F. Pei, W. C. Ren, D. M. Tang, L. B. Gao, B. L. Liu, F. Li, C. Liu and H. M. Cheng, *Adv. Mater.*, 2009, **21**, 1756–1760.
13 J. K. Wassei and R. B. Kaner, *Mater. Today*, 2010, **13**, 52–59.
14 Y. X. Huang and P. Chen, *Adv. Mater.*, 2010, **22**, 2818–2823.
15 T. Asefa, C. T. Duncan and K. K. Sharma, *Analyst*, 2009, **134**, 1980–1990.
16 Y. X. Huang, D. Cai and P. Chen, *Anal. Chem.*, 2011, **83**, 4393–4406.
17 S. Roy and Z. Q. Gao, *Nano Today*, 2009, **4**, 318–334.
18 M. F. Frasco and N. Chaniotakis, *Sensors*, 2009, **9**, 7266–7286.
19 C. P. Han and H. B. Li, *Anal. Bioanal. Chem.*, 2010, **397**, 1437–1444.
20 H. Haick, *J. Phys. D: Appl. Phys.*, 2007, **40**, 7173–7186.
21 X. L. Luo, A. Morrin, A. J. Killard and M. R. Smyth, *Electroanalysis*, 2006, **18**, 319–326.
22 K. I. Chen, B. R. Li and Y. T. Chen, *Nano Today*, 2011, **6**, 131–154.
23 F. Patolsky, G. Zheng and C. M. Lieber, *Nanomedicine*, 2006, **1**, 51–65.
24 N. S. Ramgir, Y. Yang and M. Zacharias, *Small*, 2010, **6**, 1705–1722.
25 A. K. Wanekaya, W. Chen, N. V. Myung and A. Mulchandani, *Electroanalysis*, 2006, **18**, 533–550.
26 C. B. Jacobs, M. J. Peairs and B. J. Venton, *Anal. Chim. Acta*, 2010, **662**, 105–127.
27 K. Maehashi and K. Matsumoto, *Sensors*, 2009, **9**, 5368–5378.
28 N. Sinha, J. Z. Ma and J. T. W. Yeow, *J. Nanosci. Nanotechnol.*, 2006, **6**, 573–590.
29 T. Zhang, S. Mubeen, N. V. Myung and M. A. Deshusses, *Nanotechnology*, 2008, **19**, 332001.
30 K. S. Novoselov, A. K. Geim, S. V. Morozov, D. Jiang, Y. Zhang, S. V. Dubonos, I. V. Grigorieva and A. A. Firsov, *Science*, 2004, **306**, 666–669.
31 F. N. Xia, T. Mueller, R. Golizadeh-Mojarad, M. Freitag, Y. M. Lin, J. Tsang, V. Perebeinos and P. Avouris, *Nano Lett.*, 2009, **9**, 1039–1044.
32 S. Pisana, P. M. Braganca, E. E. Marinero and B. A. Gurney, *IEEE Trans. Magn.*, 2010, **46**, 1910–1913.
33 B. Arash, Q. Wang and W. H. Duan, *Phys. Lett. A*, 2011, **375**, 2411–2415.
34 A. Sakhaee-Pour, M. T. Ahmadian and A. Vafai, *Solid State Commun.*, 2008, **145**, 168–172.
35 Y. Wang, R. Yang, Z. W. Shi, L. C. Zhang, D. X. Shi, E. Wang and G. Y. Zhang, *ACS Nano*, 2011, **5**, 3645–3650.
36 A. K. Geim and K. S. Novoselov, *Nat. Mater.*, 2007, **6**, 183–191.
37 Y. Zhang, Y.-W. Tan, H. L. Stormer and P. Kim, *Nature*, 2005, **438**, 201–204.
38 F. Schedin, A. K. Geim, S. V. Morozov, E. W. Hill, P. Blake, M. I. Katsnelson and K. S. Novoselov, *Nat. Mater.*, 2007, **6**, 652–655.
39 Y. M. Lin and P. Avouris, *Nano Lett.*, 2008, **8**, 2119–2125.
40 A. N. Pal and A. Ghosh, *Appl. Phys. Lett.*, 2009, **95**, 082105.
41 W. C. Ren, L. B. Gao, L. P. Ma and H. M. Cheng, *New Carbon Mater.*, 2011, **26**, 71–80.
42 X. C. Dong, P. Wang, W. J. Fang, C. Y. Su, Y. H. Chen, L. J. Li, W. Huang and P. Chen, *Carbon*, 2011, **49**, 3672–3678.
43 A. Reina, X. T. Jia, J. Ho, D. Nezich, H. B. Son, V. Bulovic, M. S. Dresselhaus and J. Kong, *Nano Lett.*, 2009, **9**, 30–35.
44 X. S. Li, W. W. Cai, J. H. An, S. Kim, J. Nah, D. X. Yang, R. Piner, A. Velamakanni, I. Jung, E. Tutuc, S. K. Banerjee, L. Colombo and R. S. Ruoff, *Science*, 2009, **324**, 1312–1314.
45 C. M. C. Mattevi, H. Kim and M. Chhowalla, *J. Mater. Chem.*, 2011, **21**, 3324–3334.
46 J. Hass, W. A. de Heer and E. H. Conrad, *J. Phys.: Condens. Matter*, 2008, **20**, 323202.
47 J. Kedzierski, P. L. Hsu, P. Healey, P. W. Wyatt, C. L. Keast, M. Sprinkle, C. Berger and W. A. de Heer, *IEEE Trans. Electron Devices*, 2008, **55**, 2078–2085.
48 S. Y. Zhou, G. H. Gweon, A. V. Fedorov, P. N. First, W. A. de Heer, D. H. Lee, F. Guinea, A. H. Castro Neto and A. Lanzara, *Nat. Mater.*, 2007, **6**, 770–775.
49 H. P. Boehm, A. Clauss, G. O. Fischer and U. Hofmann, *Z. Naturforsch*, 1962, **17**, 150–153.
50 D. R. Dreyer, S. Park, C. W. Bielawski and R. S. Ruoff, *Chem. Soc. Rev.*, 2010, **39**, 228–240.
51 C. D. Zangmeister, *Chem. Mater.*, 2010, **22**, 5625–5629.
52 L. J. Cote, R. Cruz-Silva and J. X. Huang, *J. Am. Chem. Soc.*, 2009, **131**, 11027–11032.
53 Y. Y. Shao, J. Wang, M. Engelhard, C. M. Wang and Y. H. Lin, *J. Mater. Chem.*, 2010, **20**, 743–748.
54 O. C. Compton and S. T. Nguyen, *Small*, 2010, **6**, 711–723.
55 Q. Y. He, S. X. Wu, S. Gao, X. H. Cao, Z. Y. Yin, H. Li, P. Chen and H. Zhang, *ACS Nano*, 2011, **5**, 5038–5044.

56 M. Pumera, *Chem. Soc. Rev.*, 2010, **39**, 4146–4157.
57 W. S. Hummers and R. E. Offeman, *J. Am. Chem. Soc.*, 1958, **80**, 1339.
58 D. C. Marcano, D. V. Kosynkin, J. M. Berlin, A. Sinitskii, Z. Z. Sun, A. Slesarev, L. B. Alemany, W. Lu and J. M. Tour, *ACS Nano*, 2010, **4**, 4806–4814.
59 K. Erickson, R. Erni, Z. Lee, N. Alem, W. Gannett and A. Zettl, *Adv. Mater.*, 2010, **22**, 4467–4472.
60 G. Eda and M. Chhowalla, *Adv. Mater.*, 2010, **22**, 2392–2415.
61 K. P. Loh, Q. L. Bao, G. Eda and M. Chhowalla, *Nat. Chem.*, 2010, **2**, 1015–1024.
62 G. Eda, C. Mattevi, H. Yamaguchi, H. Kim and M. Chhowalla, *J. Phys. Chem. C*, 2009, **113**, 15768–15771.
63 X. C. Dong, Y. M. Shi, Y. Zhao, D. M. Chen, J. Ye, Y. G. Yao, F. Gao, Z. H. Ni, T. Yu, Z. X. Shen, Y. X. Huang, P. Chen and L. J. Li, *Phys. Rev. Lett.*, 2009, **102**, 135501.
64 Y. Hernandez, V. Nicolosi, M. Lotya, F. M. Blighe, Z. Y. Sun, S. De, I. T. McGovern, B. Holland, M. Byrne, Y. K. Gun'ko, J. J. Boland, P. Niraj, G. Duesberg, S. Krishnamurthy, R. Goodhue, J. Hutchison, V. Scardaci, A. C. Ferrari and J. N. Coleman, *Nat. Nanotechnol.*, 2008, **3**, 563–568.
65 G. P. Keeley, A. O'Neill, N. McEvoy, N. Peltekis, J. N. Coleman and G. S. Duesberg, *J. Mater. Chem.*, 2010, **20**, 7864–7869.
66 X. C. Dong, C. Y. Su, W. J. Zhang, J. W. Zhao, Q. D. Ling, W. Huang, P. Chen and L. J. Li, *Phys. Chem. Chem. Phys.*, 2010, **12**, 2164–2169.
67 D. C. Wei and Y. Q. Liu, *Adv. Mater.*, 2010, **22**, 3225–3241.
68 H. T. Liu, Y. Q. Liu and D. B. Zhu, *J. Mater. Chem.*, 2011, **21**, 3335–3345.
69 J. W. Bai and Y. Huang, *Mater. Sci. Eng., R*, 2010, **70**, 341–353.
70 L. Y. Jiao, X. R. Wang, G. Diankov, H. L. Wang and H. J. Dai, *Nat. Nanotechnol.*, 2010, **5**, 321–325.
71 A. L. Higginbotham, D. V. Kosynkin, A. Sinitskii, Z. Z. Sun and J. M. Tour, *ACS Nano*, 2010, **4**, 2059–2069.
72 A. G. Cano-Marquez, F. J. Rodriguez-Macias, J. Campos-Delgado, C. G. Espinosa-Gonzalez, F. Tristan-Lopez, D. Ramirez-Gonzalez, D. A. Cullen, D. J. Smith, M. Terrones and Y. I. Vega-Cantu, *Nano Lett.*, 2009, **9**, 1527–1533.
73 L. C. Campos, V. R. Manfrinato, J. D. Sanchez-Yamagishi, J. Kong and P. Jarillo-Herrero, *Nano Lett.*, 2009, **9**, 2600–2604.
74 L. Y. Jiao, L. Zhang, X. R. Wang, G. Diankov and H. J. Dai, *Nature*, 2009, **458**, 877–880.
75 A. V. Talyzin, S. Luzan, I. V. Anoshkin, A. G. Nasibulin, H. Jiang, E. I. Kauppinen, V. M. Mikoushkin, V. V. Shnitov, D. E. Marchenko and D. Noreus, *ACS Nano*, 2011, **5**, 5132–5140.
76 D. B. Shinde, J. Debgupta, A. Kushwaha, M. Aslam and V. K. Pillai, *J. Am. Chem. Soc.*, 2011, **133**, 4168–4171.
77 K. Kim, A. Sussman and A. Zettl, *ACS Nano*, 2010, **4**, 1362–1366.
78 P. Kumar, L. S. Panchakarla and C. N. R. Rao, *Nanoscale*, 2011, **3**, 2127–2129.
79 M. Sprinkle, M. Ruan, Y. Hu, J. Hankinson, M. Rubio-Roy, B. Zhang, X. Wu, C. Berger and W. A. de Heer, *Nat. Nanotechnol.*, 2010, **5**, 727–731.
80 J. M. Cai, P. Ruffieux, R. Jaafar, M. Bieri, T. Braun, S. Blankenburg, M. Muoth, A. P. Seitsonen, M. Saleh, X. L. Feng, K. Mullen and R. Fasel, *Nature*, 2010, **466**, 470–473.
81 Z. H. Chen, Y. M. Lin, M. J. Rooks and P. Avouris, *Phys. E (Amsterdam, Neth.)*, 2007, **40**, 228–232.
82 T. Ihn, J. Guttinger, F. Molitor, S. Schnez, E. Schurtenberger, A. Jacobsen, S. Hellmuller, T. Frey, S. Droscher, C. Stampfer and K. Ensslin, *Mater. Today*, 2010, **13**, 44–50.
83 L. A. Ponomarenko, F. Schedin, M. I. Katsnelson, R. Yang, E. W. Hill, K. S. Novoselov and A. K. Geim, *Science*, 2008, **320**, 356–358.
84 C. Stampfer, E. Schurtenberger, F. Molitor, J. Guttinger, T. Ihn and K. Ensslin, *Nano Lett.*, 2008, **8**, 2378–2383.
85 D. Y. Pan, J. C. Zhang, Z. Li and M. H. Wu, *Adv. Mater.*, 2010, **22**, 734–738.
86 Y. B. Zhang, T. T. Tang, C. Girit, Z. Hao, M. C. Martin, A. Zettl, M. F. Crommie, Y. R. Shen and F. Wang, *Nature*, 2009, **459**, 820–823.
87 X. Huang, Z. Yin, S. Wu, X. Qi, Q. He, Q. Zhang, Q. Yan, F. Boey and H. Zhang, *Small*, 2011, **7**, 1876–1902.
88 W. Choi, I. Lahiri, R. Seelaboyina and Y. S. Kang, *Crit. Rev. Solid State Mater. Sci.*, 2010, **35**, 52–71.
89 D. R. Dreyer, R. S. Ruoff and C. W. Bielawski, *Angew. Chem., Int. Ed.*, 2010, **49**, 9336–9344.
90 S. J. Guo and S. J. Dong, *Chem. Soc. Rev.*, 2011, **40**, 2644–2672.
91 C. N. R. Rao, K. S. Subrahmanyam, H. Matte and A. Govindaraj, *Mod. Phys. Lett. B*, 2011, **25**, 427–451.
92 X. Cui, C. Z. Zhang, R. Hao and Y. L. Hou, *Nanoscale*, 2011, **3**, 2118–2126.
93 M. Terrones, A. R. Botello-Mendez, J. Campos-Delgado, F. Lopez-Urias, Y. I. Vega-Cantu, F. J. Rodriguez-Macias, A. L. Elias, E. Munoz-Sandoval, A. G. Cano-Marquez, J. C. Charlier and H. Terrones, *Nano Today*, 2010, **5**, 351–372.
94 P. Singh, S. Campidelli, S. Giordani, D. Bonifazi, A. Bianco and M. Prato, *Chem. Soc. Rev.*, 2009, **38**, 2214–2230.
95 B. K. Gorityala, J. M. Ma, X. Wang, P. Chen and X. W. Liu, *Chem. Soc. Rev.*, 2010, **39**, 2925–2934.
96 Y. Wang, Z. H. Li, J. Wang, J. H. Li and Y. H. Lin, *Trends Biotechnol.*, 2011, **29**, 205–212.
97 W. Yu, H. Xie, L. Chen and Y. Li, *Symposium on Photonics and Optoelectronic (SOPO)*, 2010, DOI: 10.1109/SOPO.2010.5504403.
98 Y. L. Zhao and J. F. Stoddart, *Acc. Chem. Res.*, 2009, **42**, 1161–1171.
99 B. G. Choi, H. Park, M. H. Yang, Y. M. Jung, S. Y. Lee, W. H. Hong and T. J. Park, *Nanoscale*, 2010, **2**, 2692–2697.
100 N. Mohanty and V. Berry, *Nano Lett.*, 2008, **8**, 4469–4476.
101 S. F. Hou, M. L. Kasner, S. J. Su, K. Patel and R. Cuellari, *J. Phys. Chem. C*, 2010, **114**, 14915–14921.
102 J. J. Stephenson, A. K. Sadana, A. L. Higginbotham and J. M. Tour, *Chem. Mater.*, 2006, **18**, 4658–4661.
103 L. H. Liu, M. M. Lerner and M. D. Yan, *Nano Lett.*, 2010, **10**, 3754–3756.
104 C.-Y. Hong, Y.-Z. You and C.-Y. Pan, *Polymer*, 2006, **47**, 4300–4309.
105 Y. Huang, X. Dong, Y. Liu, L.-J. Li and P. Chen, *J. Mater. Chem.*, 2011, **21**, 12358–12362.
106 Y. X. Huang, X. C. Dong, Y. M. Shi, C. M. Li, L. J. Li and P. Chen, *Nanoscale*, 2010, **2**, 1485–1488.
107 X. C. Dong, W. Huang and P. Chen, *Nanoscale Res. Lett.*, 2011, **6**, 60.
108 X. Z. Zhou, X. Huang, X. Y. Qi, S. X. Wu, C. Xue, F. Y. C. Boey, Q. Y. Yan, P. Chen and H. Zhang, *J. Phys. Chem. C*, 2009, **113**, 10842–10846.
109 S. Mao, G. H. Lu, K. H. Yu, Z. Bo and J. H. Chen, *Adv. Mater.*, 2010, **22**, 3521–3526.
110 H. Wu, J. Wang, X. H. Kang, C. M. Wang, D. H. Wang, J. Liu, I. A. Aksay and Y. H. Lin, *Talanta*, 2009, **80**, 403–406.
111 Y. Y. Shao, J. Wang, H. Wu, J. Liu, I. A. Aksay and Y. H. Lin, *Electroanalysis*, 2010, **22**, 1027–1036.
112 M. Zhou, Y. Zhai and S. Dong, *Anal. Chem.*, 2009, **81**, 5603–5613.
113 A. Ambrosi and M. Pumera, *Chem.–Eur. J.*, 2010, **16**, 10946–10949.
114 R. L. McCreery, *Chem. Rev.*, 2008, **108**, 2646–2687.
115 L. Tang, Y. Wang, Y. Li, H. Feng, J. Lu and J. Li, *Adv. Funct. Mater.*, 2009, **19**, 2782–2789.
116 X. L. Zuo, S. J. He, D. Li, C. Peng, Q. Huang, S. P. Song and C. H. Fan, *Langmuir*, 2010, **26**, 1936–1939.
117 Z. Zhong, W. Wu, D. Wang, D. Wang, J. Shan, Y. Qing and Z. Zhang, *Biosens. Bioelectron.*, 2010, **25**, 2379–2383.
118 H. F. Xu, H. Dai and G. N. Chen, *Talanta*, 2010, **81**, 334–338.
119 Q. Lu, X. C. Dong, L. J. Li and X. A. Hu, *Talanta*, 2010, **82**, 1344–1348.
120 Q. O. Zeng, J. S. Cheng, L. H. Tang, X. F. Liu, Y. Z. Liu, J. H. Li and J. H. Jiang, *Adv. Funct. Mater.*, 2010, **20**, 3366–3372.
121 W. Lv, M. Guo, M. H. Liang, F. M. Jin, L. Cui, L. J. Zhi and Q. H. Yang, *J. Mater. Chem.*, 2010, **20**, 6668–6673.
122 Q. A. Zhang, Y. Qiao, F. Hao, L. Zhang, S. Y. Wu, Y. Li, J. H. Li and X. M. Song, *Chem.–Eur. J.*, 2010, **16**, 8133–8139.
123 S. J. Guo, D. Wen, Y. M. Zhai, S. J. Dong and E. K. Wang, *ACS Nano*, 2010, **4**, 3959–3968.
124 L. Qian and X. R. Yang, *Talanta*, 2006, **68**, 721–727.
125 M. Zhou, L. Shang, B. L. Li, L. J. Huang and S. J. Dong, *Biosens. Bioelectron.*, 2008, **24**, 442–447.
126 S. J. Guo, J. Li, W. Ren, D. Wen, S. J. Dong and E. K. Wang, *Chem. Mater.*, 2009, **21**, 2247–2257.
127 Y. X. Fang, S. J. Guo, C. Z. Zhu, Y. M. Zhai and E. K. Wang, *Langmuir*, 2010, **26**, 11277–11282.

128 Y. Zhou, S. Liu, H. J. Jiang, H. Yang and H. Y. Chen, *Electroanalysis*, 2010, **22**, 1323–1328.
129 L. Y. Cao, Y. L. Liu, B. H. Zhang and L. H. Lu, *ACS Appl. Mater. Interfaces*, 2010, **2**, 2339–2346.
130 X. H. Kang, J. Wang, H. Wu, I. A. Aksay, J. Liu and Y. H. Lin, *Biosens. Bioelectron.*, 2009, **25**, 901–905.
131 C. Cai and J. Chen, *Anal. Biochem.*, 2004, **332**, 75–83.
132 X. Luo, A. J. Killard and M. R. Smyth, *Electroanalysis*, 2006, **18**, 1131–1134.
133 P. Wu, Q. A. Shao, Y. J. Hu, J. A. Jin, Y. J. Yin, H. Zhang and C. X. Cai, *Electrochim. Acta*, 2010, **55**, 8606–8614.
134 S. Alwarappan, C. Liu, A. Kumar and C. Z. Li, *J. Phys. Chem. C*, 2010, **114**, 12920–12924.
135 G. H. Zeng, Y. B. Xing, J. A. Gao, Z. Q. Wang and X. Zhang, *Langmuir*, 2010, **26**, 15022–15026.
136 C. S. Shan, H. F. Yang, J. F. Song, D. X. Han, A. Ivaska and L. Niu, *Anal. Chem.*, 2009, **81**, 2378–2382.
137 M. H. Yang, B. G. Choi, H. Park, W. H. Hong, S. Y. Lee and T. J. Park, *Electroanalysis*, 2010, **22**, 1223–1228.
138 C. S. Shan, H. F. Yang, D. X. Han, Q. X. Zhang, A. Ivaska and L. Niu, *Biosens. Bioelectron.*, 2010, **25**, 1070–1074.
139 Y. Y. Shao, S. Zhang, M. H. Engelhard, G. S. Li, G. C. Shao, Y. Wang, J. Liu, I. A. Aksay and Y. H. Lin, *J. Mater. Chem.*, 2010, **20**, 7491–7496.
140 Y. Wang, Y. Y. Shao, D. W. Matson, J. H. Li and Y. H. Lin, *ACS Nano*, 2010, **4**, 1790–1798.
141 K. J. Huang, D. J. Niu, J. Y. Sun, C. H. Han, Z. W. Wu, Y. L. Li and X. Q. Xiong, *Colloids Surf., B*, 2011, **82**, 543–549.
142 H. S. Yin, Y. L. Zhou, Q. A. Ma, S. Y. Ai, Q. P. Chen and L. S. Zhu, *Talanta*, 2010, **82**, 1193–1199.
143 M. Du, T. Yang and K. Jiao, *J. Mater. Chem.*, 2010, **20**, 9253–9260.
144 A. Ambrosi and M. Pumera, *Phys. Chem. Chem. Phys.*, 2010, **12**, 8944–8948.
145 C. X. Lim, H. Y. Hoh, P. K. Ang and K. P. Loh, *Anal. Chem.*, 2010, **82**, 7387–7393.
146 M. Muti, S. Sharma, A. Erdem and P. Papakonstantinou, *Electroanalysis*, 2011, **23**, 272–279.
147 J. Zhao, G. F. Chen, L. Zhu and G. X. Li, *Electrochem. Commun.*, 2011, **13**, 31–33.
148 Z. Wang, J. Zhang, P. Chen, X. Zhou, Y. Yang, S. Wu, L. Niu, Y. Han, L. Wang, P. Chen, F. Boey, Q. Zhang, B. Liedberg and H. Zhang, *Biosens. Bioelectron.*, 2011, **26**, 3881–3886.
149 J. Zhang, J. P. Lei, R. Pan, Y. D. Xue and H. X. Ju, *Biosens. Bioelectron.*, 2010, **26**, 371–376.
150 B. L. Su, J. A. Tang, J. X. Huang, H. H. Yang, B. Qiu, G. N. Chen and D. P. Tang, *Electroanalysis*, 2010, **22**, 2720–2728.
151 Q. Wei, K. X. Mao, D. Wu, Y. X. Dai, J. A. Yang, B. Du, M. H. Yang and H. Li, *Sens. Actuators, B*, 2010, **149**, 314–318.
152 D. Du, Z. X. Zou, Y. S. Shin, J. Wang, H. Wu, M. H. Engelhard, J. Liu, I. A. Aksay and Y. H. Lin, *Anal. Chem.*, 2010, **82**, 2989–2995.
153 M. H. Yang, A. Javadi, H. Li and S. Q. Gong, *Biosens. Bioelectron.*, 2010, **26**, 560–565.
154 X. Yu, B. Munge, V. Patel, G. Jensen, A. Bhirde, J. D. Gong, S. N. Kim, J. Gillespie, J. S. Gutkind, F. Papadimitrakopoulos and J. F. Rusling, *J. Am. Chem. Soc.*, 2006, **128**, 11199–11205.
155 G. F. Wang, H. Huang, G. Zhang, X. J. Zhang, B. Fang and L. Wang, *Anal. Methods*, 2010, **2**, 1692–1697.
156 Y. Wang, Y. M. Li, L. H. Tang, J. Lu and J. H. Li, *Electrochem. Commun.*, 2009, **11**, 889–892.
157 L. Tan, K. G. Zhou, Y. H. Zhang, H. X. Wang, X. D. Wang, Y. F. Guo and H. L. Zhang, *Electrochem. Commun.*, 2010, **12**, 557–560.
158 W. J. Hong, H. Bai, Y. X. Xu, Z. Y. Yao, Z. Z. Gu and G. Q. Shi, *J. Phys. Chem. C*, 2010, **114**, 1822–1826.
159 N. G. Shang, P. Papakonstantinou, M. McMullan, M. Chu, A. Stamboulis, A. Potenza, S. S. Dhesi and H. Marchetto, *Adv. Funct. Mater.*, 2008, **18**, 3506–3514.
160 J. Zhang, R. H. Xue, W. Y. Ong and P. Chen, *Biophys. J.*, 2009, **97**, 1371–1380.
161 R. S. Dey and C. R. Raj, *J. Phys. Chem. C*, 2010, **114**, 21427–21433.
162 L. Y. Feng, Y. Chen, J. S. Ren and X. G. Qu, *Biomaterials*, 2011, **32**, 2930–2937.
163 X. M. Wu, Y. J. Hu, J. Jin, N. L. Zhou, P. Wu, H. Zhang and C. X. Cai, *Anal. Chem.*, 2010, **82**, 3588–3596.
164 C. X. Guo, X. T. Zheng, Z. S. Lu, X. W. Lou and C. M. Li, *Adv. Mater.*, 2010, **22**, 5164–5167.
165 B. G. Choi, H. Park, T. J. Park, M. H. Yang, J. S. Kim, S. Y. Jang, N. S. Heo, S. Y. Lee, J. Kong and W. H. Hong, *ACS Nano*, 2010, **4**, 2910–2918.
166 L. Wang, X. H. Zhang, H. Y. Xiong and S. F. Wang, *Biosens. Bioelectron.*, 2010, **26**, 991–995.
167 J. Li, S. J. Guo, Y. M. Zhai and E. K. Wang, *Anal. Chim. Acta*, 2009, **649**, 196–201.
168 J. Li, S. J. Guo, Y. M. Zhai and E. K. Wang, *Electrochem. Commun.*, 2009, **11**, 1085–1088.
169 J. M. Gong, T. Zhou, D. D. Song and L. Z. Zhang, *Sens. Actuators, B*, 2010, **150**, 491–497.
170 H. J. Du, J. S. Ye, J. Q. Zhang, X. D. Huang and C. Z. Yu, *J. Electroanal. Chem.*, 2011, **650**, 209–213.
171 T. A. Gan, C. G. Hu, Z. L. Chen and S. S. Hu, *Sens. Actuators, B*, 2010, **151**, 8–14.
172 C. Wang, L. Zhang, Z. H. Guo, J. G. Xu, H. Y. Wang, K. F. Zhai and X. Zhuo, *Microchim. Acta*, 2010, **169**, 1–6.
173 X. H. Kang, J. Wang, H. Wu, J. Liu, I. A. Aksay and Y. H. Lin, *Talanta*, 2010, **81**, 754–759.
174 H. S. Yin, Q. A. Ma, Y. L. Zhou, S. Y. Ai and L. S. Zhu, *Electrochim. Acta*, 2010, **55**, 7102–7108.
175 J. A. Li, J. H. Chen, X. L. Zhang, C. H. Lu and H. H. Yang, *Talanta*, 2010, **83**, 553–558.
176 H. J. Du, J. S. Ye, J. Q. Zhang, X. D. Huang and C. Z. Yu, *Electroanalysis*, 2010, **22**, 2399–2406.
177 C. S. Shan, H. F. Yang, D. X. Han, Q. X. Zhang, A. Ivaska and L. Niu, *Biosens. Bioelectron.*, 2010, **25**, 1504–1508.
178 C. X. Guo, Z. S. Lu, Y. Lei and C. M. Li, *Electrochem. Commun.*, 2010, **12**, 1237–1240.
179 T. S. Pui, A. Agarwal, F. Ye, N. Balasubramanian and P. Chen, *Small*, 2009, **5**, 208–212.
180 T. S. Pui, A. Agarwal, F. Ye, Z. Q. Ton, Y. X. Huang and P. Chen, *Nanoscale*, 2009, **1**, 159–163.
181 T. S. Pui, A. Agarwal, F. Ye, Y. X. Huang and P. Chen, *Biosens. Bioelectron.*, 2011, **26**, 2746–2750.
182 V. Barone, O. Hod and G. E. Scuseria, *Nano Lett.*, 2006, **6**, 2748–2754.
183 M. Han, B. Ozyilmaz, Y. Zhang, P. Jarillo-Herero and P. Kim, *Phys. Status Solidi B*, 2007, **244**, 4134–4137.
184 X. C. Dong, D. L. Fu, W. J. Fang, Y. M. Shi, P. Chen and L. J. Li, *Small*, 2009, **5**, 1422–1426.
185 D. C. Wei, Y. Q. Liu, Y. Wang, H. L. Zhang, L. P. Huang and G. Yu, *Nano Lett.*, 2009, **9**, 1752–1758.
186 S. Agarwal, X. Z. Zhou, F. Ye, Q. Y. He, G. C. K. Chen, J. Soo, F. Boey, H. Zhang and P. Chen, *Langmuir*, 2010, **26**, 2244–2247.
187 M. Kalbacova, A. Broz, J. Kong and M. Kalbac, *Carbon*, 2010, **48**, 4323–4329.
188 A. Das, S. Pisana, B. Chakraborty, S. Piscanec, S. K. Saha, U. V. Waghmare, K. S. Novoselov, H. R. Krishnamurthy, A. K. Geim, A. C. Ferrari and A. K. Sood, *Nat. Nanotechnol.*, 2008, **3**, 210–215.
189 F. Chen, Q. Qing, J. L. Xia and N. J. Tao, *Chem.–Asian J.*, 2010, **5**, 2144–2153.
190 T. O. Wehling, K. S. Novoselov, S. V. Morozov, E. E. Vdovin, M. I. Katsnelson, A. K. Geim and A. I. Lichtenstein, *Nano Lett.*, 2008, **8**, 173–177.
191 H. Pinto, R. Jones, J. P. Goss and P. R. Briddon, *Phys. Status Solidi A*, 2010, **207**, 2131–2136.
192 M. Myers, J. Cooper, B. Pejcic, M. Baker, B. Raguse and L. Wieczorek, *Sens. Actuators, B*, 2011, **155**, 154–158.
193 S. Adam, E. H. Hwang, V. M. Galitski and S. Das Sarma, *Proc. Natl. Acad. Sci. U. S. A.*, 2007, **104**, 18392–18397.
194 F. Chen, J. L. Xia, D. K. Ferry and N. J. Tao, *Nano Lett.*, 2009, **9**, 2571–2574.
195 S. K. Saha, R. C. Chandrakanth, H. R. Krishnamurthy and U. V. Waghmare, *Phys. Rev. B: Condens. Matter*, 2009, **80**, 155414.
196 W. Z. Bao, F. Miao, Z. Chen, H. Zhang, W. Y. Jang, C. Dames and C. N. Lau, *Nat. Nanotechnol.*, 2009, **4**, 562–566.
197 A. L. V. de Parga, F. Calleja, B. Borca, M. C. G. Passeggi, J. J. Hinarejos, F. Guinea and R. Miranda, *Phys. Rev. Lett.*, 2008, **100**, 056807.

198 G. H. Lu, L. E. Ocola and J. H. Chen, *Nanotechnology*, 2009, **20**, 445502.
199 H. Y. Jeong, D. S. Lee, H. K. Choi, D. H. Lee, J. E. Kim, J. Y. Lee, W. J. Lee, S. O. Kim and S. Y. Choi, *Appl. Phys. Lett.*, 2010, **96**, 3432446.
200 G. H. Lu, L. E. Ocola and J. H. Chen, *Appl. Phys. Lett.*, 2009, **94**, 3086896.
201 V. Dua, S. P. Surwade, S. Ammu, S. R. Agnihotra, S. Jain, K. E. Roberts, S. Park, R. S. Ruoff and S. K. Manohar, *Angew. Chem., Int. Ed.*, 2010, **49**, 2154–2157.
202 J. D. Fowler, M. J. Allen, V. C. Tung, Y. Yang, R. B. Kaner and B. H. Weiller, *ACS Nano*, 2009, **3**, 301–306.
203 M. W. K. Nomani, R. Shishir, M. Qazi, D. Diwan, V. B. Shields, M. G. Spencer, G. S. Tompa, N. M. Sbrockey and G. Koley, *Sens. Actuators, B*, 2010, **150**, 301–307.
204 G. Ko, H. Y. Kim, J. Ahn, Y. M. Park, K. Y. Lee and J. Kim, *Curr. Appl. Phys.*, 2010, **10**, 1002–1004.
205 J. T. Robinson, F. K. Perkins, E. S. Snow, Z. Q. Wei and P. E. Sheehan, *Nano Lett.*, 2008, **8**, 3137–3140.
206 M. Shafiei, P. G. Spizzirri, R. Arsat, J. Yu, J. du Plessis, S. Dubin, R. B. Kaner, K. Kalantar-Zadeh and W. Wlodarski, *J. Phys. Chem. C*, 2010, **114**, 13796–13801.
207 L. S. Zhang, W. D. Wang, X. Q. Liang, W. S. Chu, W. G. Song, W. Wang and Z. Y. Wu, *Nanoscale*, 2011, **3**, 2458–2460.
208 J. L. Johnson, A. Behnam, S. J. Pearton and A. Ural, *Adv. Mater.*, 2010, **22**, 4877–4880.
209 E. Massera, V. La Ferrara, M. Miglietta, T. Polichetti, I. Nasti and G. Di Francia, *Chim. Oggi*, 2011, **29**, 39–41.
210 J. L. Zhang, G. X. Shen, W. J. Wang, X. J. Zhou and S. W. Guo, *J. Mater. Chem.*, 2010, **20**, 10824–10828.
211 T. V. Cuong, V. H. Pham, J. S. Chung, E. W. Shin, D. H. Yoo, S. H. Hahn, J. S. Huh, G. H. Rue, E. J. Kim, S. H. Hur and P. A. Kohl, *Mater. Lett.*, 2010, **64**, 2479–2482.
212 G. Lu, K. Yu, L. E. Ocola and J. Chen, *Chem. Commun.*, 2011, **47**, 7761–7763.
213 K. H. Yu, P. X. Wang, G. H. Lu, K. H. Chen, Z. Bo and J. H. Chen, *J. Phys. Chem. Lett.*, 2011, **2**, 537–542.
214 Y. P. Dan, Y. Lu, N. J. Kybert, Z. T. Luo and A. T. C. Johnson, *Nano Lett.*, 2009, **9**, 1472–1475.
215 B. H. Chu, J. Nicolosi, C. F. Lo, W. Strupinski, S. J. Pearton and F. Ren, *Electrochem. Solid-State Lett.*, 2011, **14**, K43–K45.
216 J. Yi, J. M. Lee and W. Il Park, *Sens. Actuators, B*, 2011, **155**, 264–269.
217 Y. Lu, B. R. Goldsmith, N. J. Kybert and A. T. C. Johnson, *Appl. Phys. Lett.*, 2010, **97**, 3483128.
218 P. K. Ang, W. Chen, A. T. S. Wee and K. P. Loh, *J. Am. Chem. Soc.*, 2008, **130**, 14392–14393.
219 Y. Ohno, K. Maehashi and K. Matsumoto, *Biosens. Bioelectron.*, 2010, **26**, 1727–1730.
220 T. Zhang, Z. G. Cheng, Y. B. Wang, Z. J. Li, C. X. Wang, Y. B. Li and Y. Fang, *Nano Lett.*, 2010, **10**, 4738–4741.
221 H. G. Sudibya, Q. Y. He, H. Zhang and P. Chen, *ACS Nano*, 2011, **5**, 1990–1994.
222 Y. Ohno, K. Maehashi, Y. Yamashiro and K. Matsumoto, *Nano Lett.*, 2009, **9**, 3318–3322.
223 Y. Ohno, K. Maehashi and K. Matsumoto, *J. Am. Chem. Soc.*, 2010, **132**, 18012–18013.
224 M. H. Yang and S. Q. Gong, *Chem. Commun.*, 2010, **46**, 5796–5798.
225 X. C. Dong, Y. M. Shi, W. Huang, P. Chen and L. J. Li, *Adv. Mater.*, 2010, **22**, 1649–1653.
226 Y. Ohno, K. Maehashi, K. Inoue and K. Matsumoto, *Japn. J. Appl. Phys.*, 2011, **50**, 070120.
227 S. Myung, A. Solanki, C. Kim, J. Park, K. S. Kim and K. B. Lee, *Adv. Mater.*, 2011, **23**, 2221–2225.
228 R. Stine, J. T. Robinson, P. E. Sheehan and C. R. Tamanaha, *Adv. Mater.*, 2010, **22**, 5297–5300.
229 T. S. Pui, H. G. Sudibya, X. N. Luan, Q. Zhang, F. Ye, Y. X. Huang and P. Chen, *Adv. Mater.*, 2010, **22**, 3199–3203.
230 N. Shao, E. Wickstrom and B. Panchapakesan, *Nanotechnology*, 2008, **19**, 465101.
231 H. G. Sudibya, J. M. Ma, X. C. Dong, S. Ng, L. J. Li, X. W. Liu and P. Chen, *Angew. Chem., Int. Ed.*, 2009, **48**, 2723–2726.
232 J. Zhang, D. L. Fu, M. B. Chan-Park, L. J. Li and P. Chen, *Adv. Mater.*, 2009, **21**, 790–793.
233 Q. Qing, S. K. Pal, B. Z. Tian, X. J. Duan, B. P. Timko, T. Cohen-Karni, V. N. Murthy and C. M. Lieber, *Proc. Natl. Acad. Sci. U. S. A.*, 2010, **107**, 1882–1887.
234 F. Patolsky, B. P. Timko, G. H. Yu, Y. Fang, A. B. Greytak, G. F. Zheng and C. M. Lieber, *Science*, 2006, **313**, 1100–1104.
235 T. Cohen-Karni, Q. Qing, Q. Li, Y. Fang and C. M. Lieber, *Nano Lett.*, 2010, **10**, 1098–1102.
236 Q. Y. He, H. G. Sudibya, Z. Y. Yin, S. X. Wu, H. Li, F. Boey, W. Huang, P. Chen and H. Zhang, *ACS Nano*, 2010, **4**, 3201–3208.
237 P. Chen and K. D. Gillis, *Biophys. J.*, 2000, **79**, 2162–2170.
238 P. Chen, T. C. Hwang and K. D. Gillis, *J. Gen. Physiol.*, 2001, **118**, 135–144.
239 Y. X. Huang, H. G. Sudibya and P. Chen, *Biosens. Bioelectron.*, 2011, **26**, 4257–4261.
240 R. Kempaiah, A. Chung and V. Maheshwari, *ACS Nano*, 2011, **5**, 6025–6031.
241 X. Zhou, J. M. Moran-Mirabal, H. G. Craighead and P. L. McEuen, *Nat. Nanotechnol.*, 2007, **2**, 185–190.
242 Y. X. Huang, P. V. Palkar, L. J. Li, H. Zhang and P. Chen, *Biosens. Bioelectron.*, 2010, **25**, 1834–1837.
243 P. K. Ang, M. Jaiswal, C. Lim, Y. Wang, J. Sankaran, A. Li, C. T. Lim, T. Wohland, O. Barbaros and K. P. Loh, *ACS Nano*, 2010, **4**, 7387–7394.
244 Z. G. Cheng, Q. Li, Z. J. Li, Q. Y. Zhou and Y. Fang, *Nano Lett.*, 2010, **10**, 1864–1868.
245 M. Dankerl, M. V. Hauf, A. Lippert, L. H. Hess, S. Birner, I. D. Sharp, A. Mahmood, P. Mallet, J. Y. Veuillen, M. Stutzmann and J. A. Garrido, *Adv. Funct. Mater.*, 2010, **20**, 3117–3124.
246 J. N. Tey, I. P. M. Wijaya, J. Wei, I. Rodriguez and S. G. Mhaisalkar, *Microfluid. Nanofluid.*, 2010, **9**, 1185–1214.
247 S. K. Min, W. Y. Kim, Y. Cho and K. S. Kim, *Nat. Nanotechnol.*, 2011, **6**, 162–165.
248 X. Dong, Q. Long, J. Wang, M. B. Chan-Park, Y. Huang, W. Huang and P. Chen, *Nanoscale*, 2011, DOI: 10.1039/c1nr11006c.
249 Y. X. Huang, H. G. Sudibya, D. L. Fu, R. H. Xue, X. C. Dong, L. J. Li and P. Chen, *Biosens. Bioelectron.*, 2009, **24**, 2716–2720.
250 L. X. Chen, S. F. Xu and J. H. Li, *Chem. Soc. Rev.*, 2011, **40**, 2922–2942.
251 D. Cai, L. Ren, H. Z. Zhao, C. J. Xu, L. Zhang, Y. Yu, H. Z. Wang, Y. C. Lan, M. F. Roberts, J. H. Chuang, M. J. Naughton, Z. F. Ren and T. C. Chiles, *Nat. Nanotechnol.*, 2010, **5**, 597–601.
252 Z. T. Luo, P. M. Vora, E. J. Mele, A. T. C. Johnson and J. M. Kikkawa, *Appl. Phys. Lett.*, 2009, **94**, 111909.
253 X. M. Sun, Z. Liu, K. Welsher, J. T. Robinson, A. Goodwin, S. Zaric and H. J. Dai, *Nano Res.*, 2008, **1**, 203–212.
254 Z. F. Liu, Q. Liu, Y. Huang, Y. F. Ma, S. G. Yin, X. Y. Zhang, W. Sun and Y. S. Chen, *Adv. Mater.*, 2008, **20**, 3924–3930.
255 J. Kim, L. J. Cote, F. Kim and J. X. Huang, *J. Am. Chem. Soc.*, 2010, **132**, 260–267.
256 J. L. Chen and X. P. Yan, *J. Mater. Chem.*, 2010, **20**, 4328–4332.
257 K. S. Subrahmanyam, P. Kumar, A. Nag and C. N. R. Rao, *Solid State Commun.*, 2010, **150**, 1774–1777.
258 L. M. Xie, X. Ling, Y. Fang, J. Zhang and Z. F. Liu, *J. Am. Chem. Soc.*, 2009, **131**, 9890–9891.
259 X. Ling, L. M. Xie, Y. Fang, H. Xu, H. L. Zhang, J. Kong, M. S. Dresselhaus, J. Zhang and Z. F. Liu, *Nano Lett.*, 2010, **10**, 553–561.
260 Z. W. Tang, H. Wu, J. R. Cort, G. W. Buchko, Y. Y. Zhang, Y. Y. Shao, I. A. Aksay, J. Liu and Y. H. Lin, *Small*, 2010, **6**, 1205–1209.
261 C. H. Lu, J. Li, J. J. Liu, H. H. Yang, X. Chen and G. N. Chen, *Chem.–Eur. J.*, 2010, **16**, 4889–4894.
262 J. W. Yi, J. Park, N. J. Singh, I. J. Lee, K. S. Kim and B. H. Kim, *Bioorg. Med. Chem. Lett.*, 2011, **21**, 704–706.
263 F. Li, Y. Huang, Q. Yang, Z. T. Zhong, D. Li, L. H. Wang, S. P. Song and C. H. Fan, *Nanoscale*, 2010, **2**, 1021–1026.
264 H. F. Dong, W. C. Gao, F. Yan, H. X. Ji and H. X. Ju, *Anal. Chem.*, 2010, **82**, 5511–5517.
265 S. Jiang, A. Liu, H. Duan, J. Soo and P. Chen, *Adv. Funct. Mater.*, 2011, **21**, 2776–2780.
266 C. H. Lu, H. H. Yang, C. L. Zhu, X. Chen and G. N. Chen, *Angew. Chem., Int. Ed.*, 2009, **48**, 4785–4787.
267 S. D. Jhaveri, R. Kirby, R. Conrad, E. J. Maglott, M. Bowser, R. T. Kennedy, G. Glick and A. D. Ellington, *J. Am. Chem. Soc.*, 2000, **122**, 2469–2473.

268 R. H. Yang, Z. W. Tang, J. L. Yan, H. Z. Kang, Y. M. Kim, Z. Zhu and W. H. Tan, *Anal. Chem.*, 2008, **80**, 7408–7413.
269 H. X. Chang, L. H. Tang, Y. Wang, J. H. Jiang and J. H. Li, *Anal. Chem.*, 2010, **82**, 2341–2346.
270 X. H. Wang, C. Y. Wang, K. G. Qu, Y. J. Song, J. S. Ren, D. Miyoshi, N. Sugimoto and X. G. Qu, *Adv. Funct. Mater.*, 2010, **20**, 3967–3971.
271 Y. Wang, Z. H. Li, D. H. Hu, C. T. Lin, J. H. Li and Y. H. Lin, *J. Am. Chem. Soc.*, 2010, **132**, 9274–9276.
272 Y. Q. Wen, F. F. Xing, S. J. He, S. P. Song, L. H. Wang, Y. T. Long, D. Li and C. H. Fan, *Chem. Commun.*, 2010, **46**, 2596–2598.
273 S. J. He, B. Song, D. Li, C. F. Zhu, W. P. Qi, Y. Q. Wen, L. H. Wang, S. P. Song, H. P. Fang and C. H. Fan, *Adv. Funct. Mater.*, 2010, **20**, 453–459.
274 B. Dubertret, M. Calame and A. J. Libchaber, *Nat. Biotechnol.*, 2001, **19**, 365–370.
275 S. Tyagi and F. R. Kramer, *Nat. Biotechnol.*, 1996, **14**, 303–308.
276 H. X. Li and L. Rothberg, *Proc. Natl. Acad. Sci. U. S. A.*, 2004, **101**, 14036–14039.
277 R. H. Yang, J. Y. Jin, Y. Chen, N. Shao, H. Z. Kang, Z. Xiao, Z. W. Tang, Y. R. Wu, Z. Zhu and W. H. Tan, *J. Am. Chem. Soc.*, 2008, **130**, 8351–8358.
278 J. Balapanuru, J. X. Yang, S. Xiao, Q. L. Bao, M. Jahan, L. Polavarapu, J. Wei, Q. H. Xu and K. P. Loh, *Angew. Chem., Int. Ed.*, 2010, **49**, 6549–6553.
279 L. P. Cai, R. Y. Zhan, K. Y. Pu, X. Y. Qi, H. Zhang, W. Huang and B. Liu, *Anal. Chem.*, 2011, **83**, 7849–7855.
280 C. L. Zhang, Y. X. Yuan, S. M. Zhang, Y. H. Wang and Z. H. Liu, *Angew. Chem., Int. Ed.*, 2011, **50**, 6851–6854.
281 X. H. Zhao, R. M. Kong, X. B. Zhang, H. M. Meng, W. N. Liu, W. H. Tan, G. L. Shen and R. Q. Yu, *Anal. Chem.*, 2011, **83**, 5062–5066.
282 Y. Q. Wen, C. Peng, D. Li, L. Zhuo, S. J. He, L. H. Wang, Q. Huang, Q. H. Xu and C. H. Fan, *Chem. Commun.*, 2011, **47**, 6278–6280.
283 F. Liu, J. Y. Choi and T. S. Seo, *Biosens. Bioelectron.*, 2010, **25**, 2361–2365.
284 J. H. Jung, D. S. Cheon, F. Liu, K. B. Lee and T. S. Seo, *Angew. Chem., Int. Ed.*, 2010, **49**, 5708–5711.
285 L. Wu, H. S. Chu, W. S. Koh and E. P. Li, *Opt. Express*, 2010, **18**, 14395–14400.
286 S. H. Choi, Y. L. Kim and K. M. Byun, *Opt. Express*, 2011, **19**, 458–466.
287 L. Wang, C. Z. Zhu, L. Han, L. H. Jin, M. Zhou and S. J. Dong, *Chem. Commun.*, 2011, **47**, 7794–7796.
288 Y. X. Xu, L. Zhao, H. Bai, W. J. Hong, C. Li and G. Q. Shi, *J. Am. Chem. Soc.*, 2009, **131**, 13490–13497.
289 Y. J. Song, K. G. Qu, C. Zhao, J. S. Ren and X. G. Qu, *Adv. Mater.*, 2010, **22**, 2206–2210.
290 Y. Wang, J. Lu, L. Tang, H. Chang and J. Li, *Anal. Chem.*, 2009, **81**, 9710–9715.
291 S. Xu, Y. Liu, T. Wang and J. Li, *Anal. Chem.*, 2011, **83**, 3817–3823.
292 G. Lu, H. Li, C. Liusman, Z. Yin, S. Wu and H. Zhang, *Chem. Sci.*, 2011, **2**, 1817–1821.
293 W. Ren, Y. X. Fang and E. K. Wang, *ACS Nano*, 2011, **5**, 6425–6433.
294 P. Chen and C. M. Li, *Small*, 2007, **3**, 1204–1208.
295 A. Meller, L. Nivon, E. Brandin, J. Golovchenko and D. Branton, *Proc. Natl. Acad. Sci. U. S. A.*, 2000, **97**, 1079–1084.
296 P. Chen, T. Mitsui, D. B. Farmer, J. Golovchenko, R. G. Gordon and D. Branton, *Nano Lett.*, 2004, **4**, 1333–1337.
297 Y. R. Kim, C. M. Li, Q. Wang and P. Chen, *Front. Biosci.*, 2007, **12**, 2978–2983.
298 C. A. Merchant, K. Healy, M. Wanunu, V. Ray, N. Peterman, J. Bartel, M. D. Fischbein, K. Venta, Z. T. Luo, A. T. C. Johnson and M. Drndic, *Nano Lett.*, 2010, **10**, 2915–2921.
299 G. F. Schneider, S. W. Kowalczyk, V. E. Calado, G. Pandraud, H. W. Zandbergen, L. M. K. Vandersypen and C. Dekker, *Nano Lett.*, 2010, **10**, 3163–3167.
300 S. Garaj, W. Hubbard, A. Reina, J. Kong, D. Branton and J. A. Golovchenko, *Nature*, 2010, **467**, 190–193.
301 D. Branton, D. W. Deamer, A. Marziali, H. Bayley, S. A. Benner, T. Butler, M. Di Ventra, S. Garaj, A. Hibbs, X. H. Huang, S. B. Jovanovich, P. S. Krstic, S. Lindsay, X. S. S. Ling, C. H. Mastrangelo, A. Meller, J. S. Oliver, Y. V. Pershin, J. M. Ramsey, R. Riehn, G. V. Soni, V. Tabard-Cossa, M. Wanunu, M. Wiggin and J. A. Schloss, *Nat. Biotechnol.*, 2008, **26**, 1146–1153.
302 T. Nelson, B. Zhang and O. V. Prezhdo, *Nano Lett.*, 2010, **10**, 3237–3242.
303 F. P. Ouyang, S. L. Peng, H. Zhang, L. B. Weng and H. Xu, *Chin. Phys. B*, 2011, **20**, 058504.
304 H. W. C. Postma, *Nano Lett.*, 2010, **10**, 420–425.
305 Y. He, R. H. Scheicher, A. Grigoriev, R. Ahuja, S. Long, Z. Huo and M. Liu, *Adv. Funct. Mater.*, 2011, **21**, 2674–2679.
306 D. E. Jiang, V. R. Cooper and S. Dai, *Nano Lett.*, 2009, **9**, 4019–4024.
307 K. Sint, B. Wang and P. Kral, *J. Am. Chem. Soc.*, 2008, **130**, 16448–16449.
308 J. O. Sofo, A. S. Chaudhari and G. D. Barber, *Phys. Rev. B: Condens. Matter*, 2007, **75**, 153401.
309 Z. P. Chen, W. C. Ren, L. B. Gao, B. L. Liu, S. F. Pei and H. M. Cheng, *Nat. Mater.*, 2011, **10**, 424–428.
310 X. Huang, X. Qi, F. Boey and H. Zhang, *Chem. Soc. Rev.*, 2012, DOI: 10.1039/C1CS15078B.
311 X. Dong, G. Xing, M. B. Chan-Park, W. Shi, N. Xiao, J. Wang, Q. Yan, T. C. Sum, W. Huang and P. Chen, *Carbon*, 2011, **49**, 5071–5078.
312 X. C. Dong, B. Li, A. Wei, X. H. Cao, M. B. Chan-Park, H. Zhang, L. J. Li, W. Huang and P. Chen, *Carbon*, 2011, **49**, 2944–2949.